Review

Recent Sensing Technologies of Imperceptible Water in Atmosphere

Moataz Mekawy and Jin Kawakita *

Electric and Elctronic Materials Field, Electrochemical Sensors Group, Research Center for Functional Materials, National Institute for Materials Science, 1-1 Namiki, Tsukuba 305-0044, Japan; MEKAWY.Moataz@nims.go.jp
* Correspondence: KAWAKITA.Jin@nims.go.jp

Abstract: Accurate detection and quantitative evaluation of environmental water in vapor and liquids state expressed as humidity and precipitation play key roles in industrial and scientific applications. However, the development of supporting tools and techniques remains a challenge. Although optical methods such as IR and LASER could detect environmental water in the air, their apparatus is relatively huge. Alternatively, solid detection field systems (SDFSs) could recently lead to a revolution in device downsizing and sensing abilities via advanced research, mainly for materials technology. Herein, we present an overview of several SDFS based sensing categories and their core materials mainly used to detect water in atmosphere, either in the vapor or liquid phase. We considered the governing mechanism in the detection process, such as adsorption/desorption, condensation/evaporation for the vapor phase, and surface attach/detach for the liquid phase. Sensing categories such as optical, chilled mirror, resistive, capacitive, gravimetric sensors were reviewed together with their designated tools such as acoustic wave, quartz crystal microbalance, IDT, and many others, giving typical examples of daily based real scientific applications.

Keywords: water in atmosphere; humidity; solid detection field systems (SDFSs); hygrometer; detection ways

1. Introduction

Environmental water content, known generally as humidity, is defined as the amount of water vapor or liquid aerosol existing in the entire environmental air. So far, it plays a key role in the daily natural processes of mankind along with scientific and industrial applications. Therefore, humidity level control represents an essential matter for a wide scope of life, for instance, in avoiding the corrosion of oil and gas supply pipes, crop diseases, vehicle clutch deterioration, mirrors and windows fogging, improper storage of food, medicine, high-tech equipment, and many others. The detection mechanism of environmental water depends mainly on its existing physical status, either with vapor or liquid phase, as shown schematically in Figure 1. On the one hand, the vapor phase status can be kept during the measurement where the adsorption/desorption mechanism predominates, leading to the detection of water molecules that are covering or stacking on the SDFS surface. Thus far, several techniques could be used to determine the water vapor content, such as optical spectroscopic techniques (IR, LASER . . . . etc.) [1]. However, such techniques require a long light path for vapor's pre-concentration, which requires a large working space. Nevertheless, they are high cost and require well-trained personnel with special skills [2]. Recent advances in materials research lead to more cheap and compact platforms such as QCM, electronic, electrochemical sensors, and many others. Beneficial use of these newly developed techniques could finally lead to the determination of the weight, volume, and mass of water molecules. On the other hand, when the status changes from water vapor to liquid, the condensation/evaporation mechanism predominates, the dew point condensation can be determined. In the liquid phase, such as fog or rain, the

attach/detach mechanism predominates. These cases finally lead to the detection of the size and number of water droplets formed on the SDFS substrate surface. Techniques used for this category required a certain threshold volume of water droplets to detect sensing. In addition, the careful determination should be realized for surface and bulk water amounts to emphasize the liquid water in the air environment and the liquid water on the target SDFS [3].
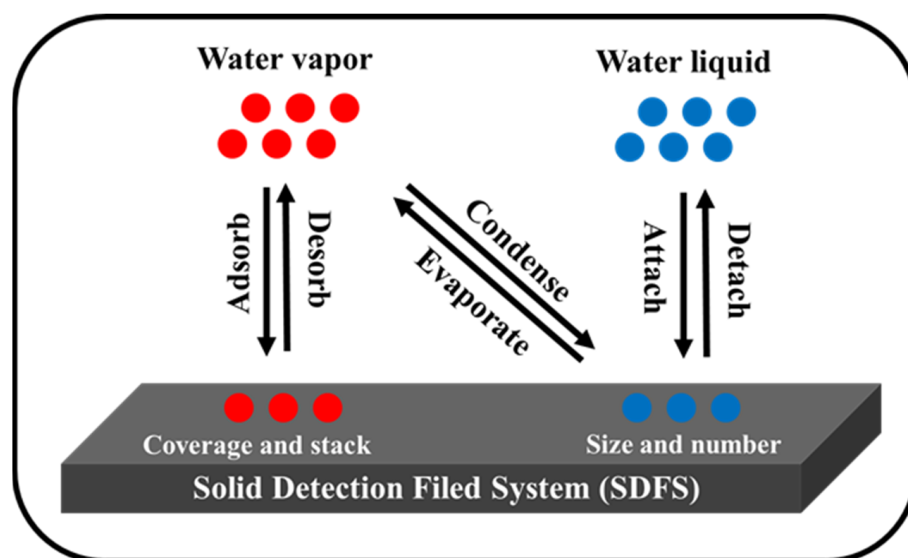
Figure 1. Schematic illustration of environmental water (humidity) detection on a solid substrate based on its physical status, related detection mechanism, and correlated output data.

In this regard, the controlled regulation of humidity implies accurate monitoring of its real level via proper sensors/actuators called "hygrometers." Historically, the first invented hygrometer was in 1450 by Nicolas Cryfts. This hygrometer used wool to determine humidity changes in the air [4–6]. Afterward, this hygrometer was modified to use a sponge instead of wool in 1550. Time by time, various modifications were carried out, changing the sensing materials to paper (Francesco Folli, 1664), human hair (Horace Bénédict de Saussure, 1783), nylon, and many others. These hygrometers were classified as mechanical hygrometers where they could record the change in humidity level based on a needle position change along the sensing materials. The first dew-point hygrometer was invented in 1820 by John Frederic Daniell and John Frederic to measure the temperature at which air becomes saturated with water molecules. A further category of hygrometers started to appear in the middle of the 19th century by Ernst Ferdinand August and Sir John Leslie, where a dry and wet-bulb psychrometer was invented. Its working mechanism depended on the evaporation of water from the wet base, which led to heat absorption affecting the level of the thermometer's reading. Correlation between these readings with various calculation tables was used to estimate the relative humidity level. This type of dew-point condensation hygrometers became the most popular model at that time. In the early 20th century, Negretti and Zambra invented a hair hygrometer or hygroscope to measure the relative humidity in the air from 10–100%. It was used to measure the relative humidity in the air with a range of 10–100% humidity depending on the existence of a bundle of hairs or other organic tissue that changes in length when it absorbs moisture. Science revolution brought many other types of hygrometers that were invented in the 20th century, such as chilled mirror hygrometers and LiCl dew point condensation (1938), and received many modifications, especially from a sensing materials viewpoint and working mechanism. However, this sensor showed slow response time and could not function beneficially in high humid environments or in the presence of ammonia or organic solvents.

In the past decade, humidity measurements received considerable attention due to the huge expansion of a wide application range such as climate change detection, food

storage conditions, oil pipes corrosion, and many others. Along with its importance in industrial activities, humidity could recently affect and beneficially control the global markets of semiconductor micro-chips fabrication, vehicle automation, healthcare goods production, and storage processes [7–12]. Especially within countries having rainy seasons, the control of humidity levels is considered mandatory. Therefore, there is a crucial need for accurate monitoring of the humidity level using updated technology for the cost-effective fabrication of humidity or moisture sensors. Thus far, there have been many efforts oriented to develop sensing methodologies. Most of them were focused on the development of sensing materials, which represents the main key of many research works. In addition, several criteria can determine the quality of the developed humidity sensor, such as its facile fabrication, economical cost, fast response time, accuracy, reliability, stability, long shelf-life time, and above all, safety. Accordingly, the application direction can be easily determined.

In general, humidity can be classified according to many expressions. The most famous or commonly used are absolute, relative and/or dew point condensation. Absolute humidity (AH) is defined as the mass of water vapor (M_V) that is existing in a certain volume of air (V). It is expressed in grams per cubic meter or the density of water vapor as in the following equation

$$AH = \frac{M_V}{V}$$

Relative humidity (RH) is usually used for a mixture of air and water. It is defined as the ratio of partial water vapor pressure (V_P) to the saturation vapor pressure of water at the same temperature (V_S). It can also be defined as the ratio of the actual existing moisture amount to the saturated amount of moisture in the atmosphere.

$$RH = \frac{V_P}{V_S}$$

Additional classification is called dew point condensation, defined as the temperature at which a totally saturated air with moisture condensation occurs. Thus, the saturation water vapor pressure is equal to the partial pressure of the water vapor (in an air atmosphere). At this point, a change in the water phase can be clearly distinguished from the vapor to liquid phase, assuming that there is no other change in the moisture content in the air. The difference between the ambient temperature and the dew point temperature is a measure of the ambient relative humidity [13]. This can be expressed as

$$T_d = T - \left(\frac{100 - RH}{5}\right)$$

where T_d is dew point temperature (in degrees Celsius), T is observed temperature (in degrees Celsius), and RH is relative humidity (in percent). This relationship is likely applicable for relative humidity values above 50% [14].

Among humidity expressions, the measurement of dew point temperature condensation (DPTC) has been internationally recognized as the most accurate relative humidity measurement method. Due to the favorable control of relative humidity level above absolute humidity, humidity sensors are most likely to measure relative humidity [13]. The working principle of dew point measurement/hygrometers is based on the passage of a certain volume of gas over a cooled substrate until condensation forms and is detected as a function of various parameters.

Humidity is considered an indirect parameter that expresses the understanding of the atmospheric water condensation process on the target surface. Recent research efforts towards humidity sensors demonstrated that they are principally designed to detect the amount of water content in the surrounding environment by monitoring the change in various parameters such as resistance, capacitance, refractive index, inductance, piezoelectric response, and many others [15–17]. In particular, resistive and capacitive sensors have received much interest due to their low cost, facile fabrication, being environmentally

benign, and ease of integration within electronic circuits that can directly enable electrical signal recording [18].

In this review, we shed light on various humidity sensing technologies based on SDFS types that are classified according to their sensing materials and working principles in a trial to better understand the conditions of surface existing water molecules. In addition, we present some of their up-to-date real feasible applications.

Our recent research works demonstrated the fabrication of a new moisture sensor based on the existence of two dissimilar Au and Al metal electrodes with a comb-like structure that possesses tailored gap size as desired. Whenever a water droplet bridges the two electrodes as a function of dew point condensation, a galvanic response current could be exclusively detected on the sensor surface with excellent sensitivity and reproducibility at a minimum response time of ~20 ms [19–27]. This criterion enabled us to beneficially use our MS in many applications, such as (1) accurate spontaneous detection of a tiny amount of water and determination of its droplet size [19–23]. (2) Improving sensor sensitivity and accuracy for dew condensation detection while changing its surface wettability [24]. (3) Enhancing the sensor's practical and scientific applicability using its surface modification according to the heat capacity of the actual target object [25,26]. (4) Achieving reliable detection methodology based on the linear relationship between response current and the variation in the sensor surface's cooling rate and the surrounding vapor pressure [22]. (5) Quantification of dew condensed water droplets on the sensor surface based on their response current and image processing techniques [27].

2. Materials for SDFSs

Hygroscopic materials are defined as materials that can absorb water molecules from the surrounding environment. They are used extensively in commercial hygrometers as a sensing layer. Previously, hair, wood, and some fabrics were used for such purposes, followed by more recent developments to achieve highly sensitive and selective materials that possess fast response/recovery criteria. Hygroscopic materials could be classified under organic, inorganic, and hybrid materials based on the materials used.

2.1. Organic Materials

Sensitive organic materials are usually marked as chemical compounds that can change their electrical or optical properties when they are subjected to air humidity or specific gases. Organic materials are frequently used for atmospheric water sensors due to their low production cost, lightweight devices, commercial availability, facile deposition on the desired substrates, and are relatively non-toxic [28]. Particularly, polymer-based humidity sensors with high sensitivity and rapid response properties have been developed [29,30]. The stability of the chosen polymer at high humidity levels could guarantee its durability and success in designated applications. The sensing mechanism is mainly recorded based on the change in conductivity or dielectric constant once the water vapor adheres to the polymeric layer. Since most of the used polymers were hydrophilic, the surface dissolution and instability of the used sensors were frequently noticed at higher humidity levels, leading to a decrease in the measurement accuracy. This, in turn, suggests the performance within a low dynamic range. The formation of crosslinked films after coating the sensitive materials on the surface of electrodes provides a feasible solution for this problem [31]. However, the control of the resultant polymeric structure becomes more difficult since these crosslinking reactions usually occur within the solid-state [32,33]. Thus far, hydrophilic polymers such as polyethyleneimine (PEI), polyethylene oxide (PEO), polyvinyl alcohol (PVA), and polyaniline (PANI) were utilized as composite sensors to obtain an improved sensitivity and response time [34–36]. As a result, an increase in the sensor's surface wettability enhanced the adherence of water molecules on its surface and consequently increased the surface conductivity. In contrast, hydrophobic polymers such as polyimide, polymethylmethacrylate (PMMA), cellulose acetate butyrate (CAB), and polyethyleneterephthalate (PET) could also be used for the manufacturing of humidity

sensors. However, the diffused water molecules on the surface of hydrophobic polymers could increase the surface permittivity, which misleads the humidity level monitoring. Nevertheless, adsorption or absorption of water molecules could lead to surface swelling, which provides more surface strain affecting their response electrical properties [13].

A further type of organic materials denoted as "phthalocyanines" represents aromatic and macrocyclic organic materials. They are quite bulky and can be easily bound to different bivalent ions such as Fe^{2+}, Zn^{2+}, Cu^{2+}, Co^{2+}, Ni^{2+} within their central cavities, affecting their physical and electrical properties. Recent studies showed that zinc phthalocyanine (ZnPc) or vanadyl 3,10,17,24-tetra-tert-butyl-1,8,15,22-tetrakis(dimethylamino)-29H,31H-phthalocyanine (VTP)-based microporous device were employed as a humidity sensing material based on the variation of their capacitance response [37,38].

2.2. Inorganic Materials

Micro-nanofabrication technology plays a very important role in providing suitable sensing inorganic materials for atmospheric water detection. Thus far, metal oxides (MOxs) such as TiO_2, In_2O_3, WO_3, ZnO, SnO_2, and many others were widely used for humidity and gas sensors due to their low cost, excellent sensing properties, flexible manufacturing in various nanostructured morphologies and geometries, facile miniaturization, and high sensitivity [39,40]. They normally possess a wide band gap enabling them to provide inherent functional properties such as high surface reactivity and electrical conductivity. In an early report discussing the morphological point of view, a thin-film sensor with nano-sized $MnWO_4$ grains showed a smaller sensitivity for humidity sensing than a thick-film sensor despite having a faster response and low-temperature coefficient [41]. Nevertheless, they could be considered promising candidates for high precision humidity sensing. However, the use of pristine (MOxs) revealed poor response and large hysteresis, which limited their application particularly in humidity sensors. Recent advances to overcome this drawback indicate that using *n*- or *p*-type semiconductor MOxs represents a promising pathway to dramatically enhance the humidity sensing ability [42,43]. Numerous research works demonstrated remarkable conductivity increases due to their interaction based on the humidity level. Their reaction mechanism could be ascribed to the molecular adsorption (by chemisorption, physisorption, or Vander Waals) of water molecules at the dangling bonds of the semiconductor surface molecules, which leads finally to a change in their electrical conductivity due to electron or hole mobility that affects the conduction and valence bands [42–44]. However, the linearity in conductivity response could be attained at lower temperatures and became non-linear once the temperature was getting higher [45–47].

Alternatively, achieving better performance towards practical sensing applications could enhance the effective sensing surface area, surface porosity, material's robustness, and signal-to-noise ratio (S/N). Thus, another category denoted as ceramic metal oxides (CMOxs) could be developed and used. Though MOxs and CMOxs share mainly the same interaction mechanism with atmospheric water, CMOxs possess numerous advantages such as superior mechanical strength, chemical resistance under various environments, high-temperature stability, large surface area, and reproducible electrical properties. Generally, CMOxs are used widely in many sensing fields such as temperature, humidity, pressure, oxygen, proximity, automobile, capacitive, oil level, and corrosion sensors [18,48].

Several reports demonstrated that CMOxs may or may not possess spinel structures. They beneficially function as sensing materials for electrochemical, mass, and optical humidity sensors due to their excellent practical robustness, stability, wide temperature range, mechanical strength, and low fabrication costs. They tend to change their electrical properties such as resistance or capacitance as a response to humidity sensing [13,49]. The sensing mechanism is governed by water adsorption on the CMOxs surface, and this process is supported by a distinctive CMOxs structure with pores, grains, and grain boundaries [50].

The interaction of water molecules with CMOxs surface leads to the formation of surface hydroxyl groups where the first ordered and stable chemisorbed water monolayer can be formed via hydrogen bonding [51,52]. Further adsorption of water molecules leads to the formation of physiosorbed layers that possess weak hydrogen bonding. The water molecules are randomly oriented on the surface of the first physiosorbed water layer allowing the proton conduction to take place by the Grotthus mechanism [53]. This, in turn, enhances the conductivity throughout the CMOxs material surface once the water molecules are more accumulated at higher relative humidity levels [54]. However, the performance of most CMOxs materials came with less sensitivity at lower relative humidity levels <20%. Sensitivity enhancement of the sensing ability could be achieved using porous CMOxs materials where the surface and open pores are likely to collect water vapor through chemical and physical adsorption, which finally leads to dew point condensation [51,52]. It was found that the pore surface conductivity and sensitivity were remarkably changed even with a small variation in the humidity. However, practical use in the atmospheric environment showed remarkable degradation due to pores blocking with undesired interfering components such as dust, dirt, oil, smoke, alcohol, or solvents.

Additionally, prolonged exposure of CMOxs materials to humid environments could lead to the formation of a stable chemisorbed hydroxyl group on their surfaces. This, in turn, provides misleading in the electrical signal outcome affecting the judge about the humidity level. However, CMOxs surface regeneration becomes possible once heated at elevated temperatures expresses a great advantage over other used materials. Thus, the design of several commercial sensors becomes likely to contain a heater for surface regeneration. However, the surface-related phenomena of humidity sensing by CMOxs materials made them have lower resistance levels than those of organic polymers towards the surface contaminations due to being mainly porous.

Furthermore, CNTs are considered extraordinary sensor candidates due to their inherent mechanical and electrical properties, facile surface functionalization, and easy integration within electronic circuits [55]. In defect-free MWCNTs, the bonds between carbon atoms in their sidewalls are sp^2 hybridized. This criterion facilitates intermolecular interactions through noncovalent van der Waals forces or π-electrons stacking [55]. Particularly MWCNTs contain both holes and electrons, and they show their metallic nature at room temperature due to the overlapping of conduction and valence bands with electrons as majority carriers. Moreover, MWCNTs can also show their semiconducting nature with the energy overlap that changes the molecular chirality [56]. To date, many research works demonstrated the use of chemically functionalized CNTs as core platforms for atmospheric water sensing [57–59]. For instance, a humidity sensor based on cellulose paper employed SWCNTs functionalized with carboxylic acid demonstrated linear behavior up to a relative humidity of 75% [60].

Further developments in the past two decades have led to the development of another category denoted as "2D materials". Thus far, 2D materials have attracted considerable attention in the sensing field due to their high specific surface area, rich-surface functionality, considerably high carrier mobility, fast response, and efficient selective detection. Graphene, reduced graphene oxide (rGO), molybdenum disulfide (MoS_2), black phosphorus, transition metal carbides and carbonitrides, and transition metal sulfides are among the typical examples of 2D materials that were used particularly for humidity sensors fabrication [61–70]. However, the agglomeration of stacked multilayers of 2D materials affected their superior sensing ability. This problem was solved by combining 2D materials with metal oxides or metallic particles to form porous structures. Apparently, 2D materials with spontaneously formed porous structures would be attractive for improving sensing performance and simplifying the preparation process [71–73].

In 2011, a new family of 2D metal carbides, nitrides, or carbonitrides, MXenes developed strong hydrophilicity and high electrical conductivity [74,75]. Thus far, $Ti_3C_2T_x$ MXenes revealed a greater conductivity along the direction of the plane than that perpendicular to the plane [76]. This criterion enabled the intercalation of water molecules

in the interlayer leading to the low electrical conductivity of water. The increase of the layer-to-layer repeating distance increased the resistance of $Ti_3C_2T_x$ [68,70,77]. Thus, these characteristics enhanced $Ti_3C_2T_x$ MXenes as a 2D material for RH sensing. Moreover, the investigation of the electrical and gravimetric response to water vapor using $Ti_3C_2T_x$ MXene films intercalated cations such as K^+ and Mg^{2+} was achieved [68]. In addition, alkalized $Ti_3C_2T_x$ were employed to enhance the gas and humidity sensing properties [77]. However, material synthesis revealed that the large stacked-layer structure inhibited water vapor diffusion, affecting the humidity sensing durability and accuracy. Further synthesis modification demonstrated the achievement of accordion-like $Ti_3C_2T_x$ MXene/$K_2Ti_4O_9$ (A-$Ti_3C_2T_x$/$K_2Ti_4O_9$) and sheet-like $Ti_3C_2T_x$ MXene/$K_2Ti_4O_9$ (S-$Ti_3C_2T_x$/$K_2Ti_4O_9$) composites as humidity sensing materials with satisfactory contact between water molecules and sensing materials [78].

2.3. Hybrid Materials

Enhancing sensing materials stability and hysteresis remains among the major challenges to achieving better sensor reliability. The future for atmospheric water sensing materials could be feasibly enhanced using hybrid structures that combine more than one of the aforementioned materials like graphene with another 2D inorganic material such as MXene. In this regard, hybrid fibers of $Ti_3C_2T_x$/graphene revealed better electrical and mechanical properties and better applications in flexible wearable sensors [79]. Furthermore, flexible SDFSs systems based on hybrid 2D materials–MoS_2 were also employed to enhance the humidity and gas sensing characteristics [62,80]. Additionally, a flexible humidity sensor based on SnO_2/reduced graphene oxide (RGO) nanocomposite film was fabricated on a flexible polyimide (PI) substrate [81]. These hybrid sensors showed better sensitivity and faster response and recovery times than traditional humidity sensors. Moreover, better results could also be achieved via the formation of a hybrid composition of organic polymers with other inorganic materials such as carbon nanotubes (CNTs) either in single-walled (SWCNTs) or multi-walled (MWCNTs) type. For instance, a hybrid film composed of poly acrylic acid (PAA) and 33 wt% of MWCNTs exhibited a volume change due to humidity adsorption and desorption, leading to an increase or a decrease in the distance between neighboring MWCNTs. Consequently, the electrical resistance of the film could be varied with the volume changes as a function of adsorption and desorption of water vapor [82]. Similarly, other hybrid materials employing polyimide (PI) [83], polyvinylpyrrolidone (PVP) [84], or polyvinyl alcohol (PVA) [85] along with CNTs could be achieved. To date, numerous research works continue towards the beneficial use of composite materials based on the hybrid structure of organic polymers and CNTs, revealing their feasibility in humidity and gas sensors [44,86].

3. Detection of Water Vapor on SDFSs

(Working Principles of Hygrometer)

The humidity sensor can be defined as an integrated electronic device that can detect and measure the degree of water vapor status on a target SDFS and convert it into a response analog signal. Thus far, humidity sensors are known as "hygrometers". A hygrometer is defined as an instrument to measure humidity. The simplest form of a hygrometer is known as a "psychrometer." It is composed of two thermometers, including dry and wet bulbs, respectively. A wet-bulb is usually used to detect the temperature where the evaporation induced by the wet bulb lowers the temperature. Therefore, the wet-bulb thermometer usually measures lower temperatures than the dry-bulb thermometer. When the air temperature is below freezing, the wet-bulb is covered with a thin isolating layer of ice and subjected to warmer than the dry bulb. Thus, the relative humidity can be estimated from the ambient temperature by the dry-bulb thermometer and the difference in temperatures between the wet-bulb and dry-bulb thermometers. Nevertheless, relative humidity can also be estimated from the psychrometric chart that correlated the wet and dry-bulb temperatures. Recent research could introduce several types of hygrometers

based on the working principles of indirect humidity monitoring via mechanical, electrical, and gravimetric detection. Summarization of different types along with their working principles is given below.

3.1. Mechanical Detection Way

Chilled-mirror condensation hygrometer represents the classical fundamentals of the mechanical category used for humidity detection, as shown in Figure 2. Its working mechanism depends on the mechano-optical detection of the dew condensation of a liquid water droplet which is formed on the chilled mirror as a function of the entire environmental humidity considering the temperature of the mirror at the optical threshold and the temperature of the surrounding air [87].
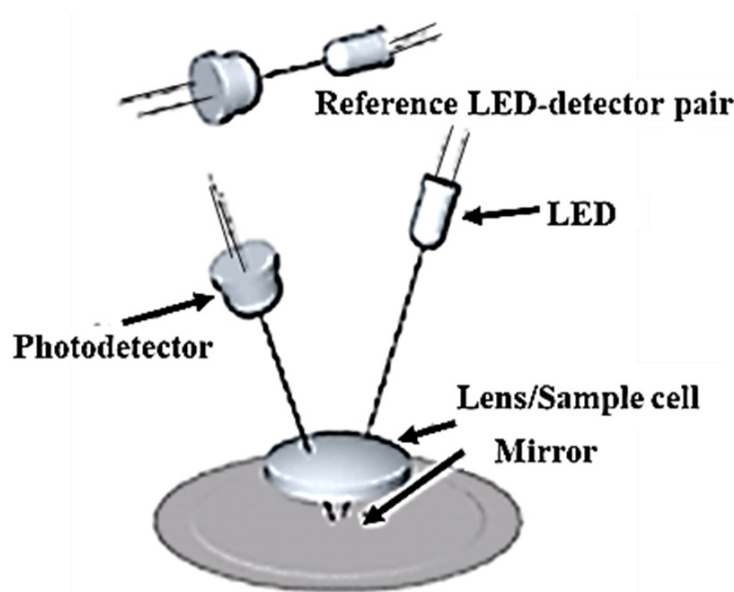
Figure 2. Chilled mirror hygrometer's working mechanism to detect dew point by cooling a reflective condensation surface until water begins to condense [87].

### 3.2. Electrical Detection Way

3.2.1. Resistive

The resistive sensing mechanism is used widely to detect humidity. It depends mainly on the ionic conductivity within the sensing layer located on the surface of the examined sensor depending on the adsorbed water molecules based on the relative humidity level. Considering the employed mechanism, either electrical response such as impedance change or mechanical response such as mechanical deformation could be achieved as a function of the detected humidity level [56].

Previous reports demonstrated that traditional resistive sensors' response times mostly range from 10 to 30 s for a 63% resistance change versus relative humidity level, which is unable to meet the requirements of real-time and rapid detection [13]. Several works of literature reported the use of different sensing materials, especially polymers, for humidity detection. However, used polymers faced limitations due to their surface instability, particularly at higher humidity levels. To overcome this, a crosslinked polymer is prepared by free radical polymerization to improve stability. Moreover, pyridine salt units have been introduced to improve stability of sensitivity as well. For instance, a rigid sulfonated polybenzimidazole sensor (SPBI) showed linear response between 20% and 95% of relative humidity [88–91]. These attempts led to the development of numerous resistive sensors with high resolution employing polymer electrolytes that possess defined structures revealing better stability, hysteresis, and linear response against humidity levels.

To date, sensing layer development continued, and several reports have shown dramatic improvements. Recently, a 2D layer of $Ti_3C_2T_x$ MXene was used for resistive humidity

detection. The surface functional group analysis of $Ti_3C_2T_x$ suggests that the ultra-fast humidity response and high sensitivity result from the high coverage rate of the hydroxyl group on the $Ti_3C_2T_x$ surface. Condensation and volatilization of water vapor molecules in accordion-like micro-structures and hierarchical nanostructures of $Ti_3C_2T_x$ lead to changes in surface electrostatic field, resulting in resistance changes of the sensor devices as shown in Figure 3 [92].
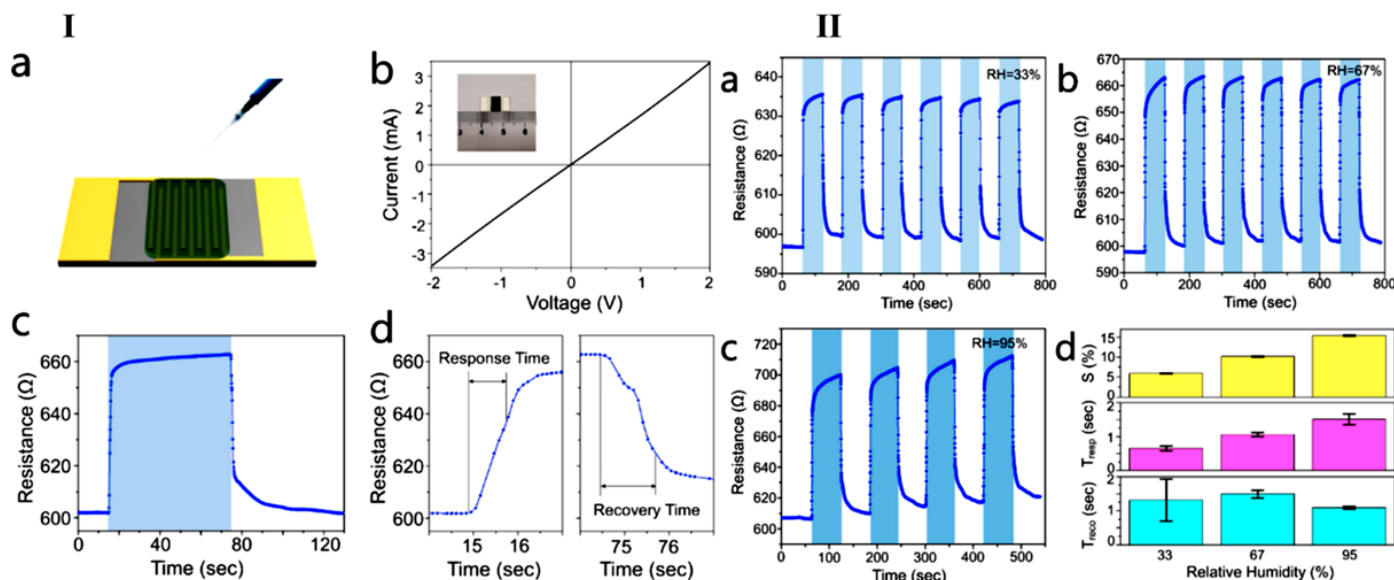
**Figure 3. I** (**a**) Schematic diagram of a humidity sensor based on layered $Ti_3C_2T_x$. (**b**) The current-voltage characteristic of the resistive humidity sensor. The inset is the optical image of the Ti3C2Tx humidity sensor device. (**c**) A typical response to 67% RH of the $Ti_3C_2T_x$ humidity sensor. (**d**) Response time (left) and recovery time (right) definition of the $Ti_3C_2T_x$ humidity sensor. **II** Repeatability of the $Ti_3C_2T_x$ humidity sensor toward (**a**) 33%, (**b**) 67%, (**c**) 95% RH at room temperature. (**d**) Average normalized responses, average response times, and recovery times plotted versus relative humidity [92].

3.2.2. Capacitive

To date, capacitive humidity sensors represent the largest market share due to their advantages over other types such as ease of fabrication, very low power consumption, high sensitivity, linear response, and above all, wide dynamic range [93]. They are mostly fabricated by depositing a thin hygroscopic layer of sensitive material from the previously mentioned categories beneath two chosen electrodes to form a capacitor-like platform. Such a platform could take sandwich-like or interdigitated (IDE) comb-like structures. The relative humidity detection mechanism using capacitive sensors depends on the change in the dielectric constant of the deposited hygroscopic sensing layer as a function of the exiting electric field between the two electrodes leading finally to generate change in capacitance [54]. In principle, the adsorption mechanism of surface water molecules with this category of humidity sensors could be elucidated as follows; water molecules interact with the surface substrate to form a complete chemisorbed monolayer. This is followed by additional physisorption of other water layers. Due to the weak bonding nature of the topmost layers, free charge transport could be generated, revealing the nature of dissociation and recombination of these surface ions. This leads to the generation of various signal outputs expressed in capacitance-related forms.

Various polymeric and ceramic candidate materials could be examined for potential use as the hygroscopic layer. However, several studies revealed that; polymeric materials were widely used due to their stability enhancement, ease of fabrication, economic fabrication cost, and better ability to form composites with extraordinary characteristics [84,94–96].

Recent reports demonstrated the use of multiple inter-digital transducer (IDT) electrodes connected in series with electrodes fabricated with PEDOT: PSS, methyl red and graphene oxide materials as multi-active sensing materials for the wide dynamic range of humidity detection, as shown in Figure 4 [97]. Full-range detection of relative humidity (0–100% RH) was examined, and the response and recovery times were 1 s and 3.5 s, respectively.
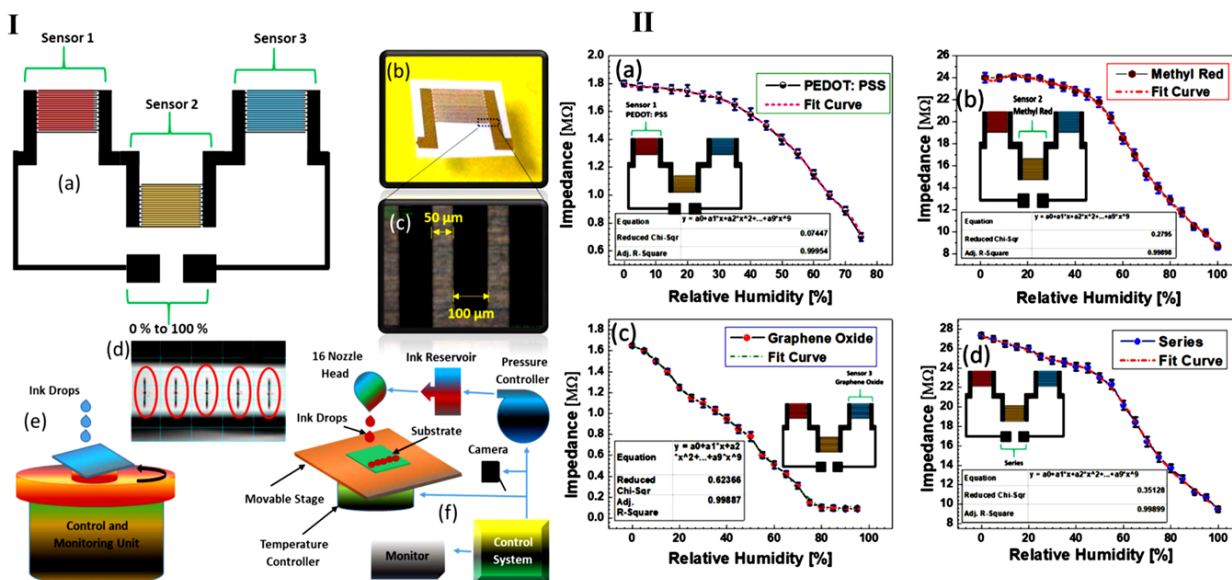
Figure 4. I (**a**) Schematic sensor image, (**b**) single fabricated inter-digital electrode, (**c**) optical image of the inter-digital electrode fingers, (**d**) stable wave shape of the ink-jet printer DMP-3000 print head, (**e**) schematic cartoon of spin coating for the active materials, and (**f**) schematic image of the ink-jet printer DMP-3000. **II** Impedance response of the sensors with (**a**) PEDOT: PSS, (**b**) methyl red, (**c**) GO thin film, and (**d**) combination of the three active sensing layers in series [97].

Further, the development of capacitive humidity sensors using naphthalene diamide derivatives (NDI) as a sensing layer was reported. Three different naphthalene diamide derivatives bearing imide side chains of different hydrophilicity were fabricated on ceramic substrates with gold interdigitated electrodes, as shown in Figure 5. They were examined for humidity sensing based on their structural morphology and thermal behavior. The response capacitance (Figure 5) was remarkably increased with the increase in humidity levels in the dynamic range between 0–95%, indicating high sensitivity, good long-term stability, excellent reproducibility, and low hysteresis than other reported capacitive sensors. However, the performance of the reported sensors from a material viewpoint is still unclear and needs more experimental investigations [98].
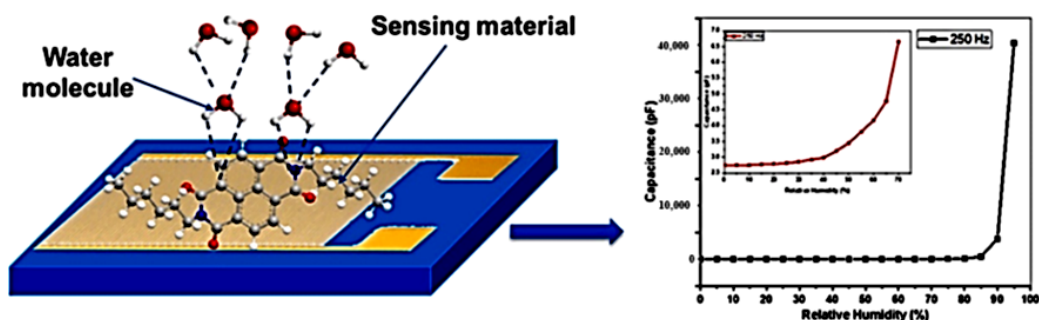
Figure 5. A schematic diagram for the sensing mechanism and the correlation between relative humidity and capacitance response [98].

Meanwhile, organic semiconductor metalloporphyrin (TDTBPPNi) was also reported to fabricate a humidity sensing layer via a microwave-assisted synthesis pathway. Experimental results revealed that; with the increase in %RH from 39 to 85%, the capacitance of the fabricated sensor had been increased by 107.37, 110.00, and 57.83 times at operational frequencies of 200 Hz, 1, and 10 kHz, respectively. However, the morphological structure of the sensing thin film layer was with amorphous and rough globular surface nature [99]. This is expected to increase the sensor surface roughness altering its surface adhesion ability which in turn affects the sensor's sensing and recovery times [100].

3.3. Optical Detection Way

Several studies demonstrated that optical humidity sensors possess more advantages than other sensor types. This could be attributed to their faster response time and their stability against created or naturally existing electric or magnetic fields. Nevertheless, they do not require any electrical contacts, which may induce components failure [101]. Early reports demonstrated that optical humidity sensors depended mainly on fluorescence and spectroscopic techniques. Their detection mechanism of humidity depended on the change in the optical properties of the sensitive sensing material core, such as photoluminescence, wavelength position, refractive index, and reflectance [102,103].

A promising fluorescent humidity sensor based on a swellable porous photonic structure was recently fabricated. It was used to investigate the correlation between the local photon density of states and the changes that occurred due to ambient conditions. Thus, creating a sensing platform that responds to relative humidity changes with well-defined, predesigned photoluminescence (PL) spectrum [104]. Figure 6 elucidates a schematic model of the fluorescent photonic humidity sensor composed of $H_3Sb_3P_2O_{14}$ nanosheets as a molecular stimuli-responsive photonic resonator sandwiched between two molecular layers of SiO_2 and TiO_2 nanoparticles. The resonator itself is composed of thin films of dyed polystyrene nanospheres that were precisely deposited at the desired depth within 2D antimony phosphate ($H_3Sb_3P_2O_{14}$) nanosheets. However, this developed sensor showed limited applicability in the real detection of environmental humidity applications beyond 75% RH level.

In addition, a novel dew point detection solution based on the integrated photonics platforms could be established. Considering the fundamentals of chilled-mirror hygrometers, this device possessed higher accuracy, a smaller footprint, and a faster response. Moreover, the cost-effective mass-productivity of photonic dew point sensor (DPS) enhances its market availability over electrical thin-film humidity sensors and chilled-mirror hygrometers [105].

Continuous progress with optical sensors development led to another category named whispering gallery mode (WGM) optical resonators humidity sensors [106]. The reaction mechanism of this category depends on their ability to confine light via total internal reflection (TIR) at their outer surface, which leads to a strong enhancement in the light interaction with the examined sensor's material. Therefore, due to humidity absorption/detection, the resonating signal change can be recognized according to the sensor's size, geometry and/or refractive index change [107,108]. Such criteria could be applied to the highly sensitive chemical and physical sensors that lead to portable and compatible miniaturization. Several types of WGM optical resonators have been reported based mainly on the existence of hygroscopic hydrophilic polymeric materials as a sensing core. This hydrophilic polymer undergoes swelling upon exposure to humidity [109]. Accordingly, the changes in refractive index and diameter of the core hygroscopic polymer result in shifting the resonant peaks with an expected high sensitivity per percent relative humidity (pm/% RH) [110,111].

In addition, several reports demonstrated the use of a polymeric WGM optical resonator doped with a fluorescent dye, demonstrating better sensitivity of 6 pm/% RH [112–114]. Some WGM sensors showed their potential applicability due to having compact laser sources. However, poor luminescence remains a challenge for non-tapered type resonators [115]. In addition, the humidity sensors have to uptake water molecules

into the resonator medium, which often disrupts the sphere's morphology or the constituent polymer's chemical integrity.
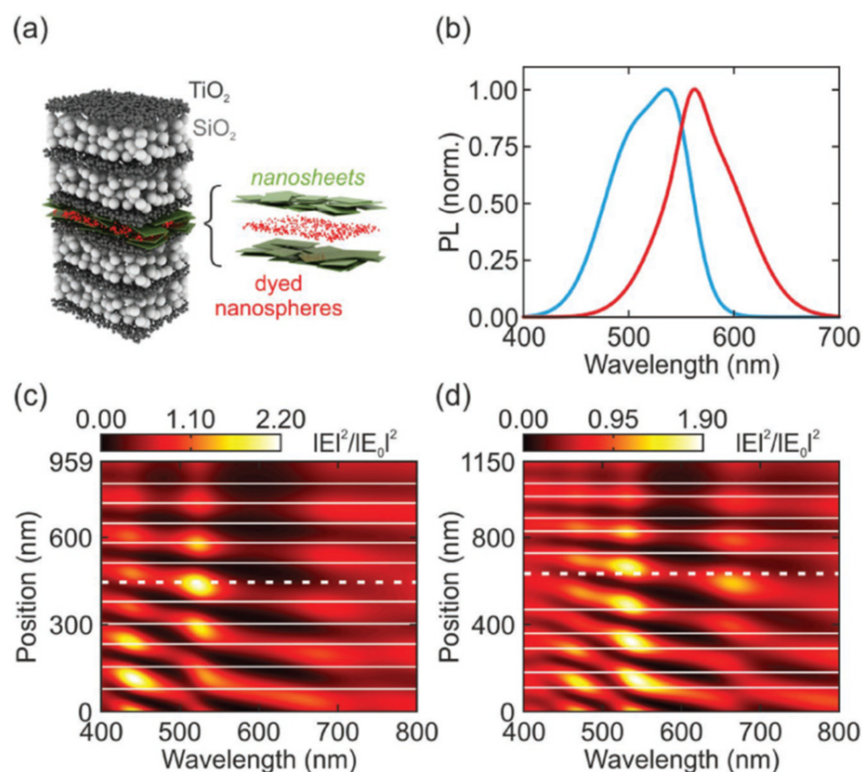
Figure 6. (**a**) Schematic model of the fluorescent photonic humidity sensor. It shows a thin emitting layer embedded in an optical cavity made of $H_3Sb_3P_2O_{14}$ nanosheets that are surrounded by two dielectric mirrors fabricated with SiO_2 and TiO_2 nanoparticles. (**b**) Excitation (blue) and emission spectra (red) of the dye molecules employed in the fluorescent sensor. Spatial and spectral distribution of the electric field intensity of the (**c**) turn-off and (**d**) turn-on samples at 0% relative humidity. Plane-wave illumination at normal incidence is assumed in the calculations. For the turn-on sample, calculations consider that the thicknesses of the SiO_2 and TiO_2 layers are 80 and 82 nm, respectively, and constant over the entire humidity range, and the optical cavity is 149 nm thick, the emitting layer being positioned in the middle of the cavity. For the turn-off sample, calculations consider that the thicknesses of the SiO_2 and TiO_2 layers are 65 and 105 nm, respectively, and the optical cavity is 260 nm thick, the emitting layer is located at a depth of one-quarter of the cavity width. Interfaces between different layers in the multilayer are indicated with thin white lines. In contrast, the position of the light-emitting layer is signaled with a white dashed line in each case [104].

Addressing these drawbacks required several modifications. Recent modifications revealed that the fabricated WGM microresonators based on an AIEgen-appended hygroscopic polymer could be a candidate for humidity sensing. The sensitivity of the PAA-TPE microsphere toward water vapor reaches 255 pm/% RH, which is considered among the highest reported non-tapered optical humidity. The working principle is shown in Figure 7. Results also revealed that the PAA-TPE microsphere maintained its humidity sensing ability through multiple swelling and de-swelling cycles. Therefore, organic luminogens based WGM water vapor sensors can be considered in the applications of miniaturized integrated optical humidity sensing devices for real-time, highly sensitive, and reliable sensing [116].

3.4. Gravimetric Detection Way

Resonance gravimetric sensing category includes quartz crystal microbalance (QCM), surface acoustic wave (SAW), film bulk acoustic resonator (FBAR), capacitive micro-machined ultrasonic transducer (CMUT), and micro-cantilever based resonator humidity

sensors [117,118]. Among the common types of physical sensors used to detect humidity are mass or gravimetric sensors, which detect changes in resonant frequency due to a mass adhered to the sensor surface by water vapor. QCM based sensors are among the widely used sensors for this purpose [119].
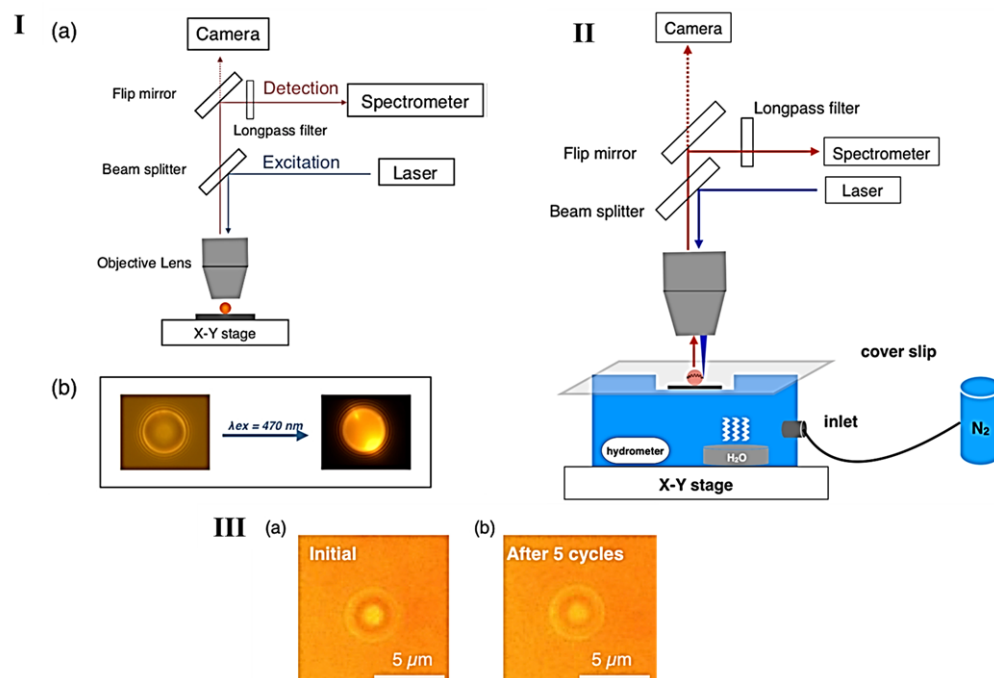
Figure 7. I (**a**) A schematic illustration of the experiment setup of μ-PL measurement. (**b**) Microscopic images of a PAA-TPE microsphere under illumination by a backlight (left) and laser excitation (right, lex = 470 nm). **II** A schematic drawing of the humidity testing setup equipped under a homemade μ-PL measurement system. **III** Microscopic images of a PAA-TPE microsphere taken before and after 5 cycles of hydration and dehydration cycles [116].

Unique criteria of mass-sensitive sensors could be attributed to their facile manufacturing and ease of operation consuming less power than other categories possessing better stability and sensitivity. QCM is mainly composed of quartz substrates with gold or silver electrodes deposited on both sides, and the sensor is mainly coated with ceramic film. The change in frequency of quartz crystal is measured, and this change depends on the adsorbed mass and films' physical properties.

Humidity mass sensors are considered assuming the easiest detection mechanism where the mass of adsorbed humid water vapor is detected and estimated. The use of Quartz Crystal Microbalance (QCM) is considered the main feature for such mass sensors where the resonating frequency change is recorded as a function of humidity change. Materials used for QCM sensors consist of quartz as a substrate coated with a sensing layer of gold, silver, or any other sensing metal oxide layer such as SnO_2 [120], $Cu(OH)_2$ [121], TiO_2 [122], graphene or carbon-based materials [123–129], polymers or composite materials [130–132].

Recent research with these materials revealed that hygroscopic dielectric cellulose and cellulose-based composites were intensively considered to sense humidity due to their large specific surface area, excellent heat resistance, and diffused double-layer structure [133,134]. Particularly, cellulose nanocrystals (CNCs) were used on a wide scale due to having a rich surface full of hygroscopic groups [135,136]. In this regard, a quartz crystal microbalance (QCM) sensor based on nitro-modified cellulose nanocrystals (NCNCs) films was developed for rapid and sensitive humidity detection. Results shown in Figure 8 demonstrated that; the humidity sensor with NCNCs load-

ing of 2.67 μg (QCM-4) exhibited high sensitivity (25.6 Hz/% RH) and relatively small response/recovery times (18 s/10 s) [137].
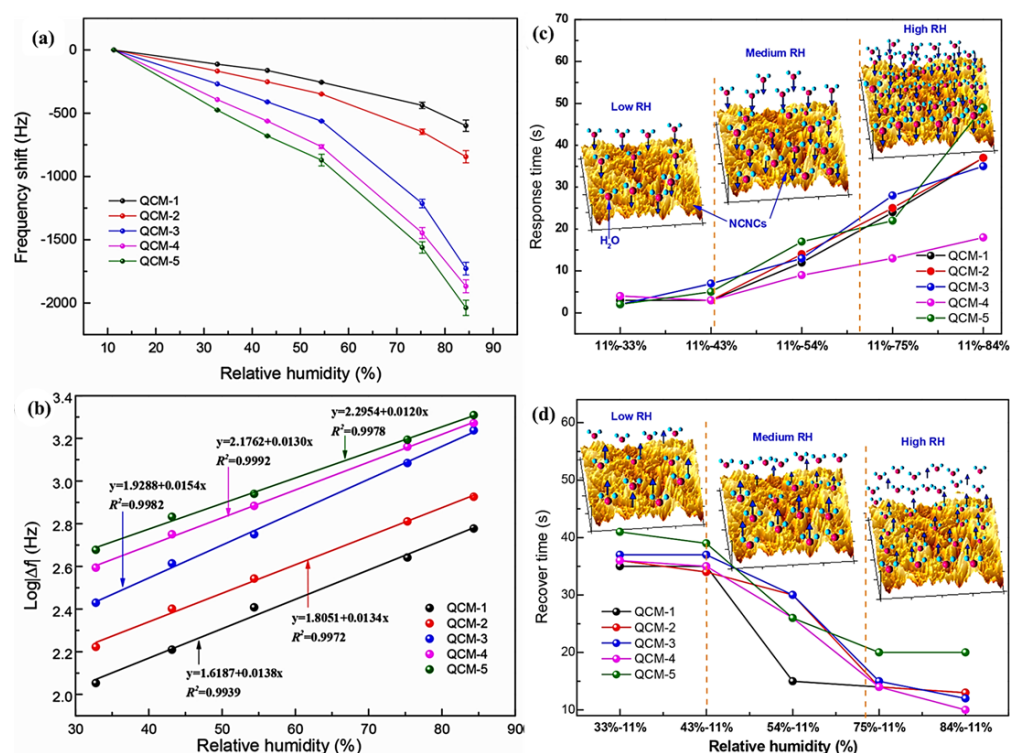
Figure 8. (**a**) Frequency shifts of sensors versus RH, (**b**) Logarithmic fitting of log|Δf| versus RH. Response time (**c**) and recovery time (**d**) of the sensors under various RH levels [137].

4. Detection of Water Liquid on SDFSs

This detection category depends mainly on the existence of an optical pathway where the gas sample passes through a metallic mirror surface that is cooled by a cooler. At a certain point, the dew condensation begins to form on the mirror surface. The amount of light reflected by the mirror diminishes, which is detected by the optical sensor. The rate of cooling can be controlled by a temperature sensor located on the mirror. Once an equilibrium is reached between the rate of evaporation and condensation, the mirror temperature represents the dew point condensation. Despite having a wide temperature range between −100 to +100 °C, it is quite expensive and requires highly skilled working personnel. In addition, it requires a very clean measurement environment and a regular high level of calibration and maintenance [138]. Such limitations could not enhance further development of chilled mirrors hygrometers for more practical and Scientific use. Figure 1 elucidates the Chilled mirror hygrometers working principle where the condensed fine water droplets are optically detected.

5. Detection of Water Vapor and Liquid on SDFSs

Our research could address the sequential detection of water molecules and water droplets. We detected the initial stage of dew condensation for such purposes using our newly developed galvanic array-based moisture sensor. As shown in Figure 9, the galvanic response current detected using different array gaps was measured as a function of controlled relative humidity. This enabled us to monitor the dew condensation event clearly while evaluating the dew point with better accuracy.

In addition, the moisture sensor output could be detected before, during, and after the dew condensation (as shown in Figures 9 and 10), which reflects the phase transition of water from tiny molecular water vapor into the liquid water droplet [23].
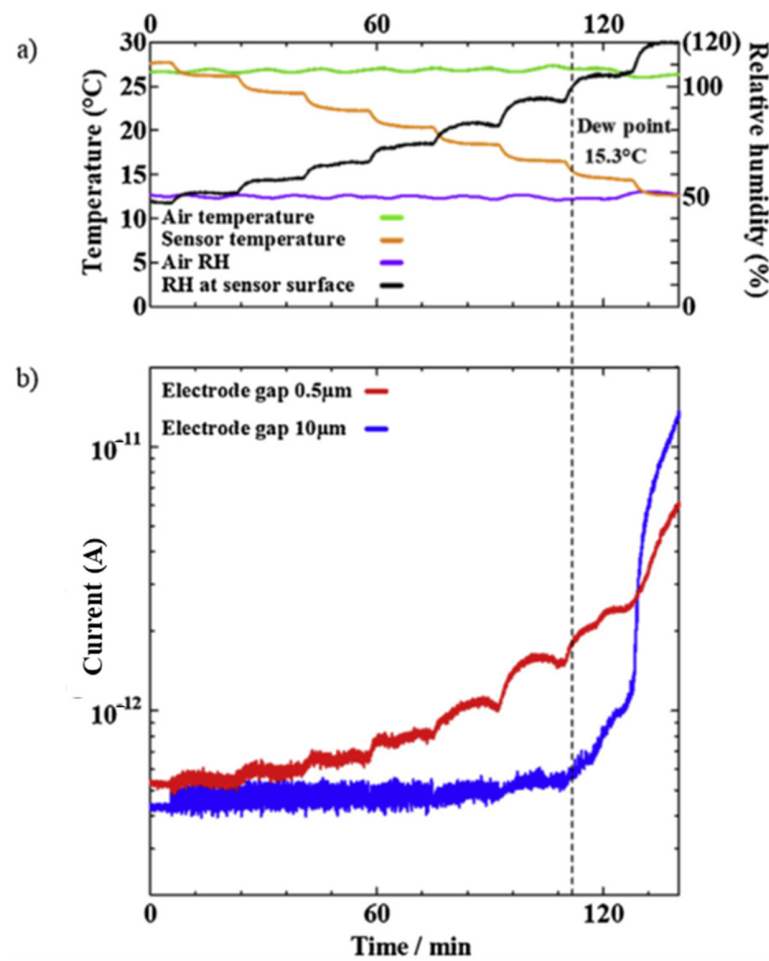
Figure 9. (**a**) Changes in temperature/relative humidity inside a test chamber and on the sensor and (**b**) sensor response as current with time when sensor surface was cooled stepwise under constant relative humidity and temperature inside test chamber [23].
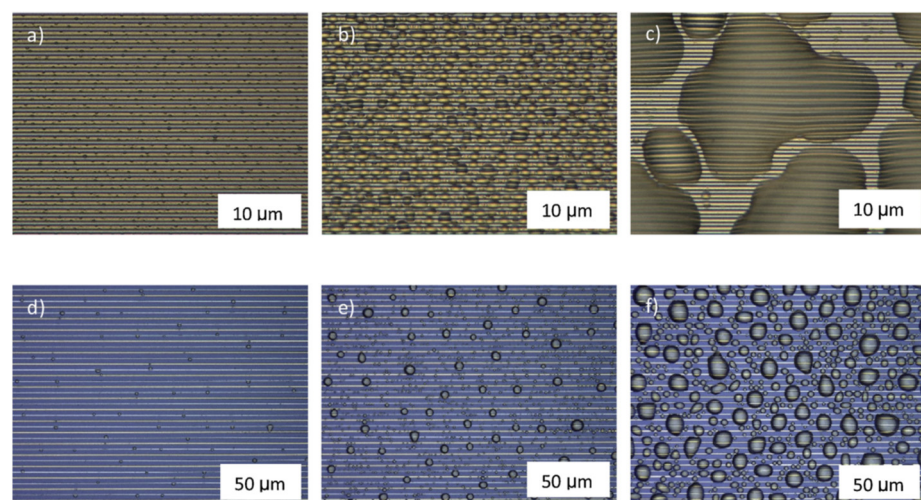
Figure 10. Microscopic images of sensor surface with 0.5 μm in array gap under (**a**) 100% (**b**) 110% and (**c**) 120% RH and with 10 μm in array gap under (**d**) 100% (**e**) 110% and(**f**) 120% RH. Value with quotation marks was indicated as nominal relative humidity, which was calculated using the humidity inside the test chamber and temperature on the sensor surface [23].

More recently and for the first time, we used electrochemical, gravimetric, and spectroscopic techniques to address the electrical response properties, mass, and nature of stacked water molecules within the interface of the sensor surface under a systematic RH controlled scheme investigating the effect of surface wettability. Figure 11 shows the simultaneously detected current and mass change per unit area as a function of relative humidity that represents the quantitative detection of water molecules before, during, and after dew condensation.
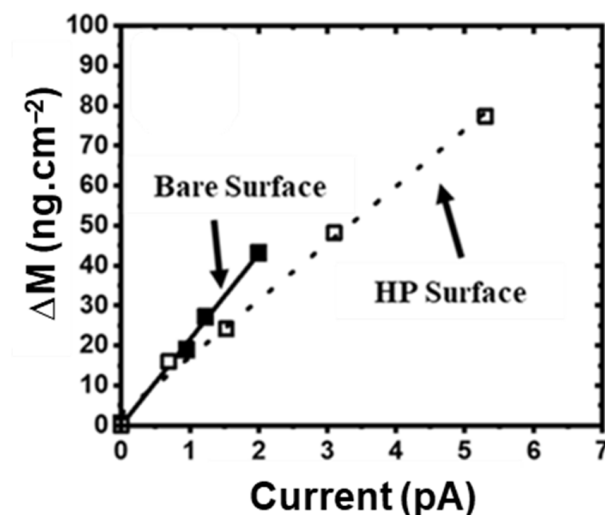
Figure 11. Calibration curves correlating the estimated mass of interfacial water molecules with response galvanic current for bare surfaces (closed rectangle) and HP coated surfaces (open rectangle) [139].

Our results demonstrated that as the number of stacked water molecules increased, the response current and frequency change were also increased. This enabled us to establish a clear quantitative estimation methodology reflecting the number of stacked water molecules on the sensor surface. Moreover, using sum frequency generation spectroscopy enabled us to reveal the nature of the interfacial water molecules based on the surface wettability of the sensors used. These experimental findings could be used to provide a promising evaluation methodology for the galvanic current arising due to stacked interfacial water molecules at different levels of RH that represents the ability to detect water either in vapor or liquid phases [139].

6. Recent Applications of Atmospheric Water Detection

6.1. Monitoring of Wound Healing

Current use of humidity sensors indicated that they are the cornerstones on which the treatment conditions and protocols could be assigned and executed. Generally, clinicians monitor the wound's status by removing the dressing, which can disturb the healing process. Wound healing is defined as an essential physiological process spontaneously done by damaged tissues to repair themselves. Careful monitoring and adjusting the wound's humidity level could affect the recovery process. If the healing process is altered, the wound suffers a risky pathologic inflammation and may become chronic and more painful [140,141]. This requires bearing more treatment costs. [142,143].

The first reported in vitro wound moisture sensor was in 2007 [144]. It was composed of two Ag/AgCl electrodes separated by silicon and enclosed within a commercial dressing. The impedance signal output was recorded as a function of the ionic nature change of the wound exudate. Thus, a correlation between the change in impedance and moisture loss was established quantitatively using different fabric types, as shown in Figure 12. This attempt opened the door for many others to enhance the detection of absorption and retention properties of different fabrics [145–147]. Furthermore, numerous studies addressed the development of resistive humidity sensors to detect wound recovery [148].
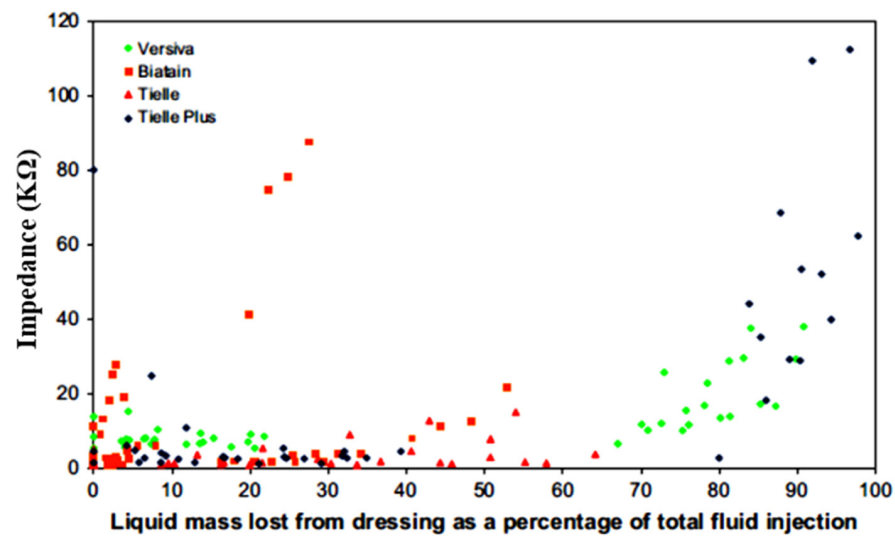
Figure 12. Relationship between the percentage of liquid lost from the dressing and the impedance measured between two silver wire electrodes embedded in the dressing using four different dressing types: Versiva, Biatain, Tielle, and Tielle Plus [144].

Recently, a new textile sensor was developed based on a screen-printed conductive polymer poly(3,4-ethylendioxythiophene): polystyrene sulfonate (PEDOT: PSS). This sensor was integrated with an RFID chip that is in turn connected within the patch employing real-time wireless monitoring of impedance change as a function of the change in the wound's moisture level, as shown in Figure 13 [149].
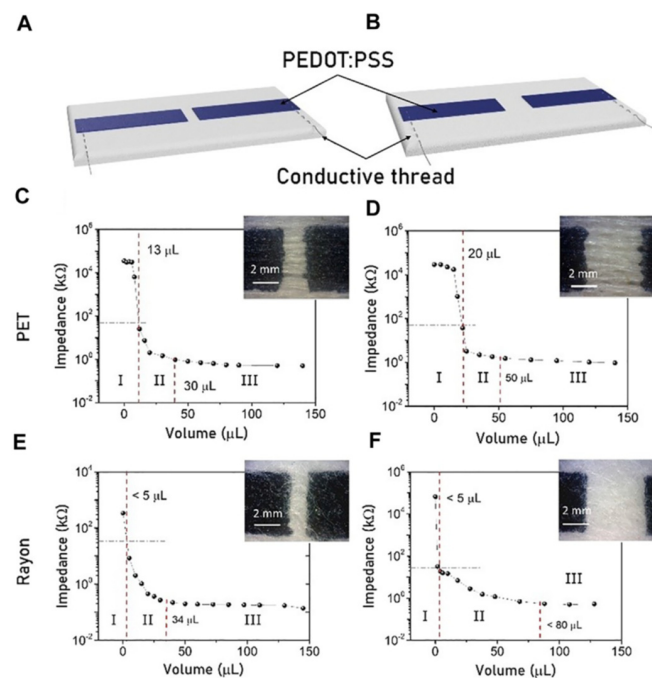

Figure 13. Impedance versus exudate volume response for moisture sensors fabricated on the gauze PET (**C**,**D**) and the gauze Rayon (**E**,**F**). Response for the different distances between the conductive electrode pads, (**A**) 2 mm and (**B**) 5 mm [149].

6.2. Greenhouse Cultivation of Crops

Greenhouse technology can provide a suitable climate for sustainable growth and cultivation of fruits and/or vegetables via an accurate control of temperature, humidity, and light conditions within a defined space of land [150].

As an example, tomatoes growth is likely to be done in relatively dry air. Previously, it was observed that RH between 55–90% does not affect the photosynthesis process giving better favorability to improve the pollen and fertilization of tomatoes between 60–70% RH. However, higher than 90% RH can stop transpiring and may lead to turgor losses in plants giving a chance to increase the pollen susceptibility to heat stress. Moreover, pests, diseases, and fungal pathogens spread rapidly and infect plants in a highly humid greenhouse environment. Some diseases may include black spot, powdery mildew, leaf-edge burn-in poinsettia, and blossom-end rot of tomatoes [151,152].

Vapor Pressure Deficit (VPD) is considered the main driving force of water movements in the plant vascular system. Thus, suitable tools and techniques are needed for its careful monitoring. Previous reports examined the effects of VPD on the transpiration rate and the plant's growth process, as shown in Figure 14 [153–156]. Enhancement of VPD regulation could improve the beneficial use of water, leading to biomass plant production and humidity-controlled storage.
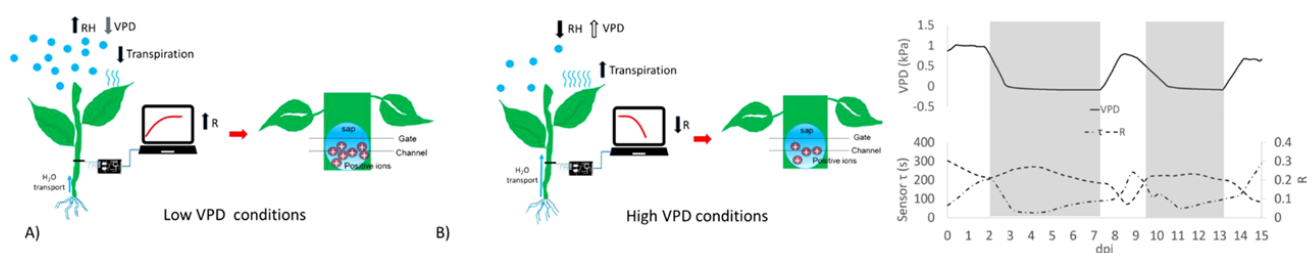
Figure 14. Scheme reporting the sensor response (R) in (**A**) low VPD conditions; (**B**) high VPD conditions. Average of R measured during the day post insertion (dpi) on all plants at Vg = 1 (dashed line), signal (dashed and pointed line), and the calculated VPD trend (solid line). Grey block indicates when the Low VPD conditions were applied [156].

6.3. Climate Forecast

Weather forecasting employs the basic principles of meteorology to collect the necessary information about temperature, humidity, and wind. It is considered an application of science technology to predict the status of the atmosphere for a prolonged time at a certain location. Therefore, humidity plays a key role in affecting the prediction of atmospheric conditions such as rainfall which depends on the equilibrium state between atmosphere and water vapor content. In other words, the prediction of rainfall depends mainly on the water vapor content and consequently on the humidity levels. Prediction of humidity on the earth's surface could be measured using similar sensors and techniques as described earlier in this review. These sensors are hung with a radiosonde in a helium balloon that is allowed to float up through the atmosphere. Communication between the radiosonde with satellites or GPS can be used to transmit and predict the amount of water vapor and the relative humidity [157]. Moreover, real and accurate humidity detection at sea or ocean sites plays a key role in predicting atmospheric disasters such as hurricanes. Using the same detection principle, buoys of several types associated with proper humidity sensors could be allocated at several sea stations and detect the wind speed and direction correlated with the temperature and humidity levels. Thus, one can estimate the surface heat flux corresponding to the sea surface [158].

7. Conclusions and Future Outlook

In summary, this review demonstrated the major categories of SDFSs sensing mechanisms, types, and perspective applications for imperceptible water in the atmosphere. For each sensing category, a literature review was presented demonstrating representative examples for the development strategy of SDFS material selection and the performance of their dependent devices. It was concluded that atmospheric water sensors shared the same understanding of fabrication strategy towards the proper development of core SDFS sensing layer to enhance the sensor's response. This response varies based on the principle,

technique, and the designated future applicability. An overview of the core sensing materials of SDFSs was classified particularly under organic, inorganic, and hybrid or composite materials. Along with the exhibited sensing parameters such as sensitivity, response time, hysteresis, and stability, it is expected that optimum sensors could be achieved. However, there still remain challenges to be addressed concerning sensors' miniaturization, circuit integration, contactless measurements, long shelf lifetime, and above all, enhancing the durability of the SDFSs core sensing materials. Future effective tackling of these challenges will guarantee the achievement of the best humidity sensors for the world needed applications.

References

1. Korotcenkov, G. Optical Hygrometers from: Handbook of Humidity Measurement. In *Methods, Materials and Technologies: Spectroscopic Methods of Humidity Measurement*; CRC Press: Boca Raton, FL, USA, 2018.
2. Wang, T.-J.; Xu, H.; Daigle, J.-F.; Sridharan, A.; Yuan, S.; Chin, S.L. Water vapor concentration measurement in air using filament-induced fluorescence spectroscopy. *Opt. Lett.* **2012**, *37*, 1706–1708. [CrossRef]
3. Tanabe, T.; Matsumoto, H.; Yudate, S.; Oyama, Y. High-Resolution Terahertz Spectroscopy of Water Vapor with Different Humidity Levels under Normal Atmospheric Conditions and in a Vapor-Liquid Coexistence at Reduced Pressure. *Biomed. J. Sci. Tech. Res.* **2018**, *10*, 7620–7624. [CrossRef]
4. Aezinia, F.; Wang, Y.; Bahreyni, B. Three dimensional touchless tracking of objects using integrated capacitive sensors. *IEEE Trans. Consum. Electron.* **2012**, *58*, 886–890. [CrossRef]
5. Wang, Y.; HajHashemi, M.S.; Bahreyni, B. A Capacitive Relative Humidity Sensor Using Polymer Nanoparticles. In Proceedings of the IEEE Sensors Conference, Taipei, Taiwan, 28–31 October 2012; pp. 418–421.
6. Bellis, M. Hygrometer History. 2006. Available online: www.inventors.about.com (accessed on 10 December 2021).
7. Faia, P.M.; Jesus, E.L.; Louro, C.S. TiO₂: WO₃ composite humidity sensors doped with ZnO and CuO investigated by impedance spectroscopy. *Sens. Actuators B Chem.* **2014**, *203*, 340–348. [CrossRef]
8. Tripathy, A.; Pramanik, S.; Manna, A.; Shasmin, H.N.; Radzi, Z.; Abu Osman, N.A. Uniformly Porous Nanocrystalline $CaMgFe_{1.33}Ti_3O_{12}$ Ceramic Derived Electro-Ceramic Nanocomposite for Impedance Type Humidity Sensor. *Sensors* **2016**, *16*, 2029. [CrossRef] [PubMed]
9. Tripathy, A.; Pramanik, S.; Manna, A.; Bhuyan, S.; Azrin Shah, N.F.; Radzi, Z.; Abu Osman, N.A. Design and Development for Capacitive Humidity Sensor Applications of Lead-Free Ca, Mg, Fe, Ti-Oxides-Based Electro-Ceramics with Improved Sensing Properties via Physisorption. *Sensors* **2016**, *16*, 1135. [CrossRef] [PubMed]
10. Dinç Zor, Ş.; Cankurtaran, H. Impedimetric Humidity Sensor Based on Nanohybrid Composite of Conducting Poly(diphenylamine sulfonic acid). *J. Sens.* **2016**, *2016*, 5479092. [CrossRef]
11. Ni, K.; Chan, C.C.; Chen, L.; Dong, X.; Huang, R.; Ma, Q. A chitosan-coated humidity sensor based on Mach-Zehnder interferometer with waist-enlarged fusion bitapers. *Opt. Fiber Technol.* **2017**, *33*, 56–59. [CrossRef]
12. Çiğil, A.B.; Cankurtaran, H.; Kahraman, M.V. Photo-crosslinked thiol-ene based hybrid polymeric sensor for humidity detection. *React. Funct. Polym.* **2017**, *114*, 75–85. [CrossRef]
13. Lee, C.-Y.; Lee, G.-B. Humidity sensors: A review. *Sens. Lett.* **2005**, *3*, 1–15. [CrossRef]
14. Lawrence, M.G. The relationship between relative humidity and the dew point temperature in moist air: A simple conversion and applications. *Bull. Am. Meteor. Soc.* **2005**, *86*, 225–233. [CrossRef]
15. Choi, K.H.; Kim, H.B.; Ali, K.; Sajid, M.; Uddin Siddiqui, G.; Chang, D.E.; Kim, H.C.; Ko, J.B.; Dang, H.W.; Doh, Y.H. Hybrid Surface Acoustic Wave- Electrohydrodynamic Atomization (SAW-EHDA) For the Development of Functional Tin Films. *Sci. Rep.* **2015**, *5*, 15178. [CrossRef]
16. Sajid, M.; Kim, H.B.; Lim, J.H.; Choi, K.H. Liquid-assisted exfoliation of 2D hBN fakes and their dispersion in PEO to fabricate highly specific and stable linear humidity sensors. *J. Mater. Chem. C* **2018**, *6*, 1421–1432. [CrossRef]

17. Siddiqui, G.U.; Sajid, M.; Ali, J.; Kim, S.W.; Doh, Y.H.; Choi, K.H. Wide range highly sensitive relative humidity sensor based on series combination of MoS$_2$ and PEDOT: PSS sensors array. *Sens. Actuators B Chem.* **2018**, *266*, 354–363. [CrossRef]
18. Krishna Prasad, N.V.; Venkata Prasad, K.; Ramesh, S.; Phanidhar, S.V.; Venkata Ratnam, K.; Janardhan, S.; Manjunatha, H.; Sarma, M.; Srinivas, K. Ceramic Sensors: A mini-review of their applications. *Front. Mater.* **2020**, *7*, 593342. [CrossRef]
19. Kawakita, J.; Chikyow, T. Detection of Micro/Nano Droplet by Galvanic-Coupled Arrays. *ECS Trans.* **2017**, *75*, 51–59. [CrossRef]
20. Kubota, Y.; Satoh, N.; Mekawy, M.; Sakamoto, Y.; Kawakita, J. Control of Heat Capacity of Moisture Sensor by Galvanic Arrays with Micro/Nano Gap toward Accurate Detection of Dew Condensation on Target. *J. Electrochem. Soc.* **2021**, *168*, 067522. [CrossRef]
21. Terada, E.; Mekawy, M.; Sakamoto, Y.; Kawakita, J. Relation between Water Status on Micro/Nano Gap between Galvanic Arrays and Flowing Current Around 100% in Relative Humidity. *J. Electrochem. Soc.* **2021**, *168*, 047512. [CrossRef]
22. Shrestha, R.G.; Kubota, Y.; Sakamoto, Y.; Kawakita, J. Quick and Sensitive Detection of Water Using Galvanic-Coupled Arrays with a Submicron Gap for the Advanced Prediction of Dew Condensation. *Sensors* **2020**, *20*, 3314. [CrossRef]
23. Mishra, V.L.; Kubota, Y.; Sakamoto, Y.; Kawakita, J. Micro/nano galvanic-coupled arrays for early and initial detection and prediction of dew condensation. *Sens. Actuators A* **2020**, *303*, 111838.
24. Shrestha, R.G.; Ando, T.; Sakamoto, Y.; Kawakita, J. Enhancement of sensitivity and accuracy of micro/nano water droplets detection using galvanic-coupled arrays. *Sensors* **2019**, *19*, 4500. [CrossRef] [PubMed]
25. Kawakita, J. Condensation Detection Element. WO 2020100778A1, 11 December 2020.
26. Shrestha, R.G.; Kawakita, J. Superhydrophilic polymer modified galvanic array moisture sensor chip with stable/improved lifetime towards enhanced dew condensation detection. *Sens. Actuators A Phys.* **2021**, *331*, 113036. [CrossRef]
27. Mekawy, M.; Terada, E.; Inoue, S.; Sakamoto, Y.; Kawakita, J. Quantitative Correlation of Droplet on Galvanic-Coupled Arrays with Response Current by Image Processing. *ACS Omega* **2021**, *6*, 30818–30825. [CrossRef]
28. Sakai, Y.; Sadaoka, Y.; Matsuguchi, M. Humidity sensors based on polymer thin films. *Sens. Actuators B* **1996**, *35*, 85–90. [CrossRef]
29. Lin, Q.Q.; Li, Y.; Yang, M.J. Investigations on the sensing mechanism of humidity sensors based on electrospun polymer nanofibers. *Sens. Actuators B* **2012**, *171*, 309–314. [CrossRef]
30. Kim, M.-J.; Gong, M.-S. Water-resistive humidity sensor prepared by printing process using polyelectrolyte ink derived from new monomer. *Analyst* **2012**, *137*, 1487–1494. [CrossRef]
31. Fei, T.; Jiang, K.; Liu, S.; Zhang, T. Humidity sensor based on a cross-linked porous polymer with unexpectedly good properties. *RSC Adv.* **2014**, *4*, 21429. [CrossRef]
32. Wang, X.; Ding, B.; Yu, J.; Wang, M. Highly sensitive humidity sensors based on electro-spinning/netting a polyamide 6 nano-fiber/net modified by polyethyleneimine. *J. Mater. Chem.* **2011**, *21*, 16231–16238. [CrossRef]
33. Gong, M.-S.; Kim, J.-U.; Kim, J.-G. Preparation of water-durable humidity sensor by attachment of polyelectrolyte membrane to electrode substrate by photochemical crosslinking reaction. *Sens. Actuators B* **2010**, *147*, 539–547. [CrossRef]
34. Wang, Y.; Wang, J.; Shao, Y.; Liao, C.; Wang, Y. Highly Sensitive Surface Plasmon Resonance Humidity Sensor Based on a Polyvinyl-Alcohol-Coated Polymer Optical Fiber. *Biosensors* **2021**, *11*, 461. [CrossRef]
35. Wang, Y.; Shen, C.; Lou, W.; Shentu, F. Fiber optic humidity sensor based on the graphene oxide/PVA composite film. *Opt. Commun.* **2016**, *372*, 229–234. [CrossRef]
36. Vu, D.L.; Li, Y.-Y.; Lin, T.-H.; Wu, M.-C. Fabrication and humidity sensing property of UV/ozone treated PANI/PMMA electrospun fibers. *J. Taiwan Inst. Chem. Eng.* **2019**, *99*, 250–257. [CrossRef]
37. Safian, N.A.M.; Anuar, A.; Omar, A.-Z.; Bawazeer, T.M.; Alsenany, A.; Alsoufi, M.S.; Supangat, A.; Roslan, N.A. Enhanced sensitivity of zinc phthalocyanine-based microporous humidity sensors by varying size of electrode gaps. *Sens. Actuators B Chem.* **2021**, *343*, 130158. [CrossRef]
38. Roslan, N.A.; Abu Bakar, A.; Bawazeer, T.M.; Alsoufi, M.S.; Alsenany, N.; Majid, W.H.A.; Supangat, A. Enhancing the performance of vanadyl phthalocyanine-based humidity sensor by varying the thickness. *Sens. Actuators B Chem.* **2019**, *279*, 148–156. [CrossRef]
39. Neri, G. First Fifty Years of Chemoresistive Gas Sensors. *Chemosensors* **2015**, *3*, 1–20. [CrossRef]
40. Nikolic, M.V.; Milovanovic, V.; Zorka, Z.; Vasiljevic, Z.Z.; Stamenkovic, Z. Semiconductor Gas Sensors: Materials, Technology, Design, and Application. *Sensors* **2020**, *20*, 6694. [CrossRef] [PubMed]
41. Qu, W.; Wlodarski, W.; Meyer, J.-U. Comparative study on micromorphology and humidity sensitive properties of thin-film and thick-film humidity sensors based on semiconducting MnWO$_4$. *Sens. Actuators B* **2000**, *64*, 76–82. [CrossRef]
42. Dwiputra, M.A.; Fadhila, F.; Imawan, G.; Fauzia, V. The enhanced performance of capacitive-type humidity sensors based on ZnO nanorods/WS$_2$ nanosheets heterostructure. *Sens. Actuators B Chem.* **2020**, *310*, 127810. [CrossRef]
43. Tsuruoka, T.; Hasegawa, T.; Terabe, K.; Aono, M. Operating mechanism and resistive switching characteristics of two- and three-terminal atomic switches using a thin metal oxide layer. *J. Electroceramics* **2017**, *39*, 143–156. [CrossRef]
44. Tulliani, J.-M.; Inserra, B.; and Ziegler, D. Carbon-Based Materials for Humidity Sensing: A Short Review. *Micromachines* **2019**, *10*, 232. [CrossRef]
45. Wang, C.; Huang, H.; Zhang, M.-R.; Song, W.-X.; Zhang, L.; Xi, R.; Wang, L.-J.; Pan, G.-B. A ZnO/porous GaN heterojunction and its application as a humidity sensor. *Nanoscale Adv.* **2019**, *1*, 1232–1239. [CrossRef]
46. Khan, M.U.; Hassan, G.; Awais, M.; Bae, J. All printed full range humidity sensor based on Fe$_2$O$_3$. Sens. *Actuators A Phys.* **2020**, *2020*, 112072. [CrossRef]

47.   Furqan, C.M.; Khan, M.U.; Awais, M.; Jiang, F.; Bae, J.; Hassan, A.; Kwok, H.-S. Humidity sensor based on Gallium Nitride for real time monitoring applications. *Sci. Rep.* **2021**, *11*, 11088. [CrossRef] [PubMed]

48.   Yadav, A. Classification and Applications of Humidity Sensors: A Review. *Int. J. Res. Appl. Sci. Eng. Technol.* **2018**, *6*, 3686. [CrossRef]

49.   Blank, T.A.; Eksperiandova, L.P.; Belikov, K.N. Recent trends of ceramic humidity sensors development: A review. *Sens. Actuators B* **2016**, *228*, 416–442. [CrossRef]

50.   Faia, P.M.; Furtado, C.S. Effect of composition on electrical response to humidity of TiO_2: ZnO sensors investigated by impedance spectroscopy. *Sens. Actuators B* **2013**, *181*, 720–729. [CrossRef]

51.   McCafferty, E.; Zettlemoyer, A.C. Adsorption of water vapor on alpha-Fe_2O_3. *Discuss. Faraday Soc.* **1971**, *52*, 239–254. [CrossRef]

52.   Morimoto, T.; Nagao, M.; Tokuda, F. Relation between the amounts of chemisorbed and physisorbed water on metal oxides. *J. Phys. Chem.* **1969**, *73*, 243–248. [CrossRef]

53.   De Grotthuss, C.J.T. Memoir on the decomposition of water and of the bodies that it holds in solution by means of galvanic electricity. *Biochim. Biophys. Acta* **2006**, *1757*, 871–875. [CrossRef]

54.   Farahani, H.; Wagiran, R.; Hamidon, M.N. Humidity sensors principle, mechanism, and fabrication technologies: A comprehensive review. *Sensors* **2014**, *14*, 7881–7939. [CrossRef]

55.   Fennell, J.F., Jr.; Liu, S.F.; Azzarelli, J.M.; Weis, J.G.; Rochat, S.; Mirica, K.A.; Ravnsbæk, J.B.; Swager, T.M. Nanowire chemical/biological sensors: Status and a roadmap for the future. *Angew. Chem. Int. Ed.* **2016**, *55*, 1266–1281. [CrossRef]

56.   Tang, Q.Y.; Chan, Y.C.; Zhang, K. Fast response resistive humidity sensitivity of polyimide/multiwall carbon nanotube composite films. *Sens. Actuators B Chem.* **2011**, *152*, 99–106. [CrossRef]

57.   Cao, C.L.; Hu, C.G.; Fang, L.; Wang, S.X.; Tian, Y.S.; Pan, C.Y. Humidity sensor based on multi-walled carbon nanotube thin films. *J. Nanomater.* **2011**, *2011*, 707303. [CrossRef]

58.   Chikkadi, K.; Muoth, M.; Liu, W.; Maiwald, V.; Hierold, C. Enhanced signal-to-noise ratio in pristine, suspended carbon nanotube gas sensors. *Sens. Actuators B Chem.* **2014**, *196*, 682–690. [CrossRef]

59.   Lee, D.; Ye, Z.; Campbell, S.A.; Cui, T. Suspended and highly aligned carbon nanotube thin-film structures using open microfluidic channel template. *Sens. Actuators A Phys.* **2012**, *188*, 434–441. [CrossRef]

60.   Han, J.-W.; Kim, B.; Li, J.; Meyyappan, M. Carbon Nanotube Based Humidity Sensor on Cellulose Paper. *J. Phys. Chem. C* **2012**, *116*, 22094–22097. [CrossRef]

61.   Zhang, D.; Tong, J.; Xia, B.; Xue, Q. Ultrahigh performance humidity sensor based on layer-by-layer self-assembly of graphene oxide/polyelectrolyte nanocomposite film. *Sens. Actuator. B Chem.* **2014**, *203*, 263–270. [CrossRef]

62.   Zhao, J.; Li, N.; Guangyu, Z.; Wei, Z.; Liao, M.; Chen, P.; Wang, S.; Shi, D.; Sun, Q.; Zhang, G. Highly sensitive MoS_2 humidity sensors array for noncontact sensation. *Adv. Mater.* **2017**, *29*, 1702076. [CrossRef]

63.   Miao, J.; Cai, L.; Zhang, S.; Nah, J.; Yeom, J.; Wang, C. Air-stable humidity sensor using few-layer black phosphorus. *ACS Appl. Mater. Interfaces* **2017**, *9*, 10019–10026. [CrossRef]

64.   Erande, M.B.; Pawar, M.S.; Late, D.J. Humidity sensing and photodetection behavior of electrochemically exfoliated atomically thin-layered black phosphorus nanosheets. *ACS Appl. Mater. Interfaces* **2016**, *8*, 11548–11556. [CrossRef]

65.   Borini, S.; White, R.; Wei, D.; Astley, M.; Haque, S.; Spigone, E.; Harris, N.; Kivioja, J.; Ryhänen, T. Ultrafast graphene oxide humidity sensors. *ACS Nano* **2013**, *7*, 11166–11173. [CrossRef] [PubMed]

66.   Shankar, S.S.; Shereema, R.M.; Rakhi, R.B. Electrochemical determination of adrenaline using MXene/graphite composite paste electrodes. *ACS Appl. Mat. Interfaces* **2018**, *10*, 43343–43351. [CrossRef] [PubMed]

67.   Yasaei, P.; Behranginia, A.; Foroozan, T.; Asadi, M.; Kim, K.; Khalili-Araghi, F.; Salehi-Khojin, A. Stable and selective humidity sensing using stacked black phosphorus flakes. *ACS Nano* **2015**, *9*, 9898–9905. [CrossRef] [PubMed]

68.   Muckley, E.S.; Naguib, M.; Wang, H.-W.; Vlcek, L.; Osti, N.C.; Sacci, R.L.; Sang, X.; Unocic, R.R.; Xie, Y.; Tyagi, M.; et al. Multimodality of structural, electrical, and gravimetric responses of intercalated MXenes to water. *ACS Nano* **2017**, *11*, 11118–11126. [CrossRef] [PubMed]

69.   Park, S.Y.; Kim, Y.H.; Lee, S.Y.; Sohn, W.; Lee, J.E.; Kim, D.H.; Shim, Y.-S.; Kwon, K.C.; Choi, K.S.; Yoo, H.J.; et al. Highly selective and sensitive chemoresistive humidity sensors based on rGO/MoS2 van der Waals composites. *J. Mater. Chem. A Mater. Energy Sustain.* **2018**, *6*, 5016–5024. [CrossRef]

70.   Muckley, E.S.; Naguib, M.; Ivanov, I.N. Multi-modal, ultrasensitive, wide-range humidity sensing with Ti_3C_2 film. *Nanoscale* **2018**, *10*, 21689–21695. [CrossRef]

71.   Natu, V.; Clites, M.; Pomerantseva, E.; Barsoum, M.W. Mesoporous MXene powders synthesized by acid induced crumpling and their use as Na-ion battery anodes. *Mater. Res. Lett.* **2018**, *6*, 230–235. [CrossRef]

72.   Zhao, M.-Q.; Xie, X.; Ren, C.E.; Makaryan, T.; Anasori, B.; Wang, G.; Gogotsi, Y. Hollow MXene spheres and 3D macroporous MXene frameworks for Na-ion storage. *Adv. Mater.* **2017**, *29*, 1702410. [CrossRef]

73.   Lipatov, A.; Alhabeb, M.; Lukatskaya, M.R.; Boson, A.; Gogotsi, Y.A. Effect of synthesis on quality, electronic properties and environmental stability of individual monolayer Ti_3C_2 MXene flakes. *Adv. Electron. Mater.* **2016**, *2*, 1600255. [CrossRef]

74.   Naguib, M.; Kurtoglu, M.; Presser, V.; Lu, J.; Niu, J.; Heon, M.; Hultman, L.; Gogotsi, Y.; Barsoum, M.W. Two-dimensional nanocrystals produced by exfoliation of Ti_3AlC_2. *Adv. Mater.* **2011**, *23*, 4248–4253. [CrossRef]

75.   Zhao, Q.-N.; Zhang, Y.-J.; Duan, Z.-H.; Wang, S.; Liu, C.; Jiang, Y.-D.; Tai, H.-L. A review on $Ti_3C_2T_x$-based nanomaterials: Synthesis and applications in gas and humidity sensors. *Rare Met.* **2021**, *40*, 1459–1476. [CrossRef]

76. Celerier, S.; Hurand, S.; Garnero, C.; Morisset, S.; Benchakar, M.; Habrioux, A.; Chartier, P.; Mauchamp, V.; Findling, N.; Lanson, B.; et al. Ferrage, Hydration of $Ti_3C_2T_x$ MXene: An interstratification process with major implications on physical properties. *Chem. Mater.* **2019**, *31*, 454–461. [CrossRef]

77. Yang, Z.; Liu, A.; Wang, C.; Liu, F.; He, J.; Li, S.; Wang, J.; You, R.; Yan, X.; Sun, P.; et al. Improvement of gas and humidity sensing properties of organ-like MXene by alkaline treatment. *ACS Sens.* **2019**, *4*, 1261–1269. [CrossRef] [PubMed]

78. Wu, J.; Lu, P.; Dai, J.; Zheng, C.; Zhang, T.; William, W.Y.; Zhang, Y. High performance humidity sensing property of $Ti_3C_2T_x$ MXene-derived $Ti_3C_2T_x$ /$K_2Ti_4O_9$ composites. *Sens. Actuators B. Chem.* **2021**, *326*, 128969. [CrossRef]

79. Lee, S.H.; Eom, W.; Shin, H.; Ambade, R.B.; Bang, J.H.; Kim, H.W.; Han, T.H. Room temperature, highly durable Ti3C2TxMXene/Graphene hybrid fibers for NH_3 gas sensing. *ACS Appl. Mater. Interfaces* **2020**, *12*, 9. [CrossRef]

80. Shen, J.; Yang, Z.; Wang, Y.; Xu, L.; Liu, R.; Liu, X. The gas sensing performance of borophene/MoS_2 heterostructure. *Appl. Sci.* **2020**, *504*, 144412. [CrossRef]

81. Zhang, D.; Chang, H.; Li, P.; Liu, R.; Xue, Q. Fabrication and characterization of an ultrasensitive humidity sensor based on metal oxide/graphene hybrid nanocomposite. *Sens. Actuators B Chem.* **2016**, *225*, 233–240. [CrossRef]

82. Lee, J.; Cho, D.; Jeong, Y. A resistive-type sensor based on flexible multi-walled carbon nanotubes and polyacrylic acid composite films. *Solid State Electron.* **2013**, *87*, 80–84. [CrossRef]

83. Yoo, K.P.; Lima, L.-T.; Min, N.-K.; Lee, M.J.; Lee, C.J.; Park, C.-W. Novel resistive-type humidity sensor based on multiwall carbon nanotube/polyimide composite films. *Sens. Actuators B Chem.* **2010**, *145*, 120–125. [CrossRef]

84. Pan, X.; Xue, Q.; Zhang, J.; Guo, Q.; Jin, Y.; Lu, W.; Li, X.; Ling, C. Effective enhancement of humidity sensing characteristics of novel thermally treated MWCNTs/Polyvinylpyrrolidone film caused by interfacial effect. *Adv. Mater. Interfaces* **2016**, *3*, 1600153. [CrossRef]

85. Zhou, G.; Byun, J.H.; Oh, Y.; Jung, B.-M.; Cha, H.-J.; Seong, D.G.; Um, M.K.; Hyun, S.; Chou, T.W. High sensitive wearable textile-based humidity sensor made of high-strength, single-walled carbon nanotube (SWCNT)/Poly(Vinyl Alcohol) (PVA) filaments. *ACS Appl. Mater. Interfaces* **2017**, *9*, 4788–4797. [CrossRef] [PubMed]

86. Barmpakos, D.; Kaltsas, G. A Review on Humidity, Temperature and Strain Printed Sensors—Current Trends and Future Perspectives. *Sensors* **2021**, *21*, 739. [CrossRef] [PubMed]

87. Beaubien, D.J. The Chilled Mirror Hygrometer: How It Works, Where It Works-and Where It Doesn't. 1 May 2005 1:00 am. Available online: https://www.fierceelectronics.com/components/chilled-mirror-hygrometer-how-it-works-where-it-works-and-where-it-doesn-t (accessed on 15 December 2021).

88. Fei, T.; Dai, J.; Jiang, K.; Zhao, H.; Zhang, T. Stable crosslinked amphiphilic polymers from a one-pot reaction for application in humidity sensors. *Sens. Actuators B Chem.* **2016**, *227*, 649–654. [CrossRef]

89. Park, K.-J.; Gong, M.-S. A water durable resistive humidity sensor based on rigid sulfonated polybenzimidazole and their properties. *Sens. Actuators B Chem.* **2017**, *246*, 53–60. [CrossRef]

90. Fei, T.; Zhao, H.; Jiang, K.; Zhang, T. Synthesis and humidity sensitive property of cross-linked water-resistant polymer electrolytes. *Sens. Actuators B Chem.* **2015**, *208*, 277–282. [CrossRef]

91. Zhuang, Z.; Li, Y.; Qi, D.; Zhao, C.; Na, H. Novel polymeric humidity sensors based on sulfonated poly (ether ether ketone) s: Influence of sulfonation degree on sensing properties. *Sens. Actuators B Chem.* **2017**, *242*, 801–809. [CrossRef]

92. Zhang, C.; Zhang, Y.; Cao, K.; Guo, Z.; Han, Y.; Hu, W.; Wu, Y.; She, Y.; He, Y. Ultrasensitive and reversible room-temperature resistive humidity sensor based on layered two-dimensional titanium carbide. *Ceram. Int.* **2021**, *47*, 6463–6469. [CrossRef]

93. Kim, J.; Cho, J.-H.; Lee, H.-M.; Hong, S.-M. Capacitive Humidity Sensor Based on Carbon Black/Polyimide Composites. *Sensors* **2021**, *21*, 1974. [CrossRef]

94. Boudaden, J.; Steinmaßl, M.; Endres, H.; Drost, A.; Eisele, I.; Kutter, C.; Müller-Buschbaum, P. Polyimide-Based Capacitive Humidity Sensor. *Sensors* **2018**, *18*, 1516. [CrossRef]

95. Peng, X.; Chu, J.; Aldalbahi, A.; Rivera, M.; Wang, L.; Duan, S.; Feng, P. A Flexible Humidity Sensor Based on KC–MWCNTs Composites. *Appl. Surf. Sci.* **2016**, *387*, 149–154. [CrossRef]

96. Fei, T.; Jiang, K.; Jiang, F.; Mu, R.; Zhang, T. Humidity Switching Properties of Sensors Based on Multiwalled Carbon Nanotubes/Polyvinyl Alcohol Composite Films. *J. Appl. Polym. Sci.* **2014**, *131*, 39726. [CrossRef]

97. Hassan, G.; Sajid, M.; Choi, C. Highly Sensitive and Full Range Detectable Humidity Sensor using PEDOT: PSS, Methyl Red and Graphene Oxide Materials. *Sci. Rep.* **2019**, *9*, 15227. [CrossRef]

98. Ali, S.; Jameel, M.A.; Gupta, A.; Langford, S.J.; Shafiei, M. Capacitive humidity sensing performance of naphthalene diimide derivatives at ambient temperature. *Synth. Met.* **2021**, *275*, 116739. [CrossRef]

99. Farooq, Z.; Yaseen, M.; Zulfqar, M.; Mahmood, M.H.R.; Akram, R.; Qadir, K.W.; Zafar, Q. Investigation of relative humidity-sensing performance of capacitive and resistive type sensor based on TDTBPPNi metalloporphyrin dielectric layer. *Bull. Mater. Sci.* **2021**, *44*, 156. [CrossRef]

100. Colak, A.; Wormeester, H.; Zandvliet, H.J.W.; Poelsema, B. Surface adhesion and its dependence on surface roughness and humidity measured with a flat tip. *Appl. Surf. Sci.* **2012**, *258*, 6938–6942. [CrossRef]

101. Wales, D.J.; Parker, R.M.; Gates, J.C.; Grossel, M.C.; Smith, P.G.R. An investigation into relative humidity measurement using an aluminosilicate sol-gel thin film as the active layer in an integrated optical Bragg grating refractometer. *Sensor. Actuator. B Chem.* **2013**, *188*, 857–866. [CrossRef]

102. Zhang, Y.; Chen, Y.; Zhang, Y.; Cheng, X.; Feng, C.; Chen, L. A novel humidity sensor based on NaTaO$_3$ nanocrystalline. *Sens. Actuators B* **2012**, *174*, 485–489. [CrossRef]

103. Jen, Y.-J.; Lin, M.-J.; Chao, J.-H. Single dielectric columnar thin film as a humidity sensor. *Sens. Actuators B* **2010**, *149*, 67–70. [CrossRef]

104. Szendrei, K.; Jiménez-Solano, A.; Lozano, G.; Lotsch, B.V.; Hernán, M. Fluorescent Humidity Sensors Based on Photonic Resonators. *Adv. Opt. Mater.* **2017**, *5*, 1700663. [CrossRef]

105. Tao, J.; Luo, Y.; Wang, L.; Cai, H.; Sun, T.; Song, J.; Liu, H.; Gu, Y. An ultrahigh-accuracy Miniature Dew Point Sensor based on an Integrated Photonics Platform. *Sci. Rep.* **2016**, *6*, 29672. [CrossRef] [PubMed]

106. Ma, Q.; Huang, L.; Guo, Z.; Rossmann, T. Spectral shift response of optical whispering-gallery modes due to water vapor adsoption and desorption. *Meas. Sci. Technol.* **2010**, *21*, 115206. [CrossRef]

107. Oki, O.; Kushida, S.; Mikosch, A.; Hatanaka, K.; Takeda, Y.; Minakata, S.; Kuwabara, J.; Kanbara, T.; Dao, T.D.; Ishii, S.; et al. FRET-mediated near infrared whispering gallery modes: Studies on the relevance of intracavity energy transfer with Q.-factors. *Mater. Chem. Front.* **2018**, *2*, 270–274. [CrossRef]

108. Zhu, N.-S.; Shi, B.-F.; Guo, Y.-Y.; Han, B.; Zhang, Y.-N. Polydimethylsiloxane self-assembled whispering gallery mode microbottle resonator for ethanol sensing. *Opt. Mater.* **2020**, *107*, 110024. [CrossRef]

109. Cai, L.; Pan, J.; Zhao, Y.; Wang, J.; Xiao, S. Whispering Gallery Mode Optical Microresonators: Structures and Sensing Applications, Phys. Status Solidi. *Appl. Mater. Sci.* **2020**, *217*, 1900825.

110. Ascorbe, J.; Corres, J.M.; Arregui, F.J.; Matias, I.R. Recent Developments in Fiber Optics Humidity Sensors. *Sensors* **2017**, *17*, 893. [CrossRef]

111. Mallik, A.K.; Farrell, G.; Liu, D.; Kavungal, V.; Wu, Q.; Semenova, Y. Whispering gallery mode micro resonators for multi-parameter sensing applications. *J. Light Technol.* **2018**, *36*, 2667–2674. [CrossRef]

112. Xu, W.; Xu, C.; Qin, F.; Shan, Y.; Zhu, Z.; Zhu, Y. Whispering-gallery mode lasing from polymer microspheres for humidity sensing. *Chin. Opt. Lett.* **2018**, *16*, 081401. [CrossRef]

113. Petermann, A.B.; Hildebrandt, T.; Morgner, U.; Roth, B.W.; Meinhardt-Wollweber, M. Polymer Based Whispering Gallery Mode Humidity Sensor. *Sensors* **2018**, *18*, 2383. [CrossRef]

114. Huang, Q.; Xu, H.; Li, M.; Hou, Z.; Lv, C.; Zhan, X.; Li, H.; Xia, H.; Wang, H.; Sun, H. Stretchable PEGDA Hydrogel-Based Whispering-Gallery-Mode Microlaser with Humidity Responsiveness. *J. Light Technol.* **2018**, *36*, 819–824. [CrossRef]

115. Andreiuk, B.; Reisch, A.; Bernhardt, E.; Klymchenko, A.S. Fighting Aggregation-Caused Quenching and Leakage of Dyes in Fluorescent Polymer Nanoparticles: Universal Role of Counter ion. *Chem. Asian J.* **2019**, *14*, 836–846. [CrossRef]

116. Qiagedeer, A.; Yamagishi, H.; Sakamoto, M.; Hasebe, H.; Ishiwari, F.; Fukushima, T.; Yamamoto, Y. A highly sensitive humidity sensor based on an aggregation-induced emission luminogen-appended hygroscopic polymer micro resonator. *Mater. Chem. Front.* **2021**, *5*, 799–803. [CrossRef]

117. Wasisto, H.S.; Merzsch, S.; Waag, A.; Uhde, E.; Salthammer, T.; Peiner, E. Airborne engineered nanoparticle mass sensor based on a silicon resonant cantilever. *Sens. Actuators B Chem.* **2013**, *180*, 77–89. [CrossRef]

118. Xu, J.; Bertke, M.; Wasisto, H.S.; Peiner, E. Piezoresistive microcantilevers for humidity sensing. *J. Micromech. Microeng.* **2019**, *29*, 053003. [CrossRef]

119. Reglero Ruiz, J.A.; Sanjuán, A.M.; Vallejos, S.; García, F.C.; García, J.M. Smart Polymers in Micro and Nano Sensory Devices. *Chemosensors* **2018**, *6*, 12. [CrossRef]

120. Gao, N.; Li, H.-Y.; Zhang, W.; Zhang, Y.; Zeng, Y.; Zhixiang, H.; Liu, J.; Jiang, J.; Miao, L.; Yi, F.; et al. QCM-based humidity sensor and sensing properties employing colloidal SnO$_2$ nanowires. *Sens. Actuators B Chem.* **2019**, *293*, 129–135. [CrossRef]

121. Lin, J.; Gao, N.; Liu, J.; Hu, Z.; Fang, H.; Tan, X.; Li, H.; Jiang, H.; Liu, H.; Shi, T.; et al. Superhydrophilic Cu(OH)$_2$ nanowires based QCM transducer with self-healing ability for humidity detection. *J. Mater. Chem. A* **2019**, *7*, 9068–9077. [CrossRef]

122. Zhang, D.; Chen, H.; Li, P.; Wang, P.; Yang, Z. Humidity sensing properties of metal organic framework-derived hollow ball-like TiO$_2$ coated QCM sensor. *IEEE Sens. J.* **2019**, *19*, 2909–2915. [CrossRef]

123. Lee, S.W.; Choi, B.I.; Kim, J.C.; Woo, S.B.; Kim, Y.G.; Yoo, Y.; Seo, Y.S. Reduction and compensation of humidity measurement errors at cold temperatures using dual QCM humidity sensors based on graphene oxides. *Sens. Actuators B Chem.* **2019**, *284*, 386–394. [CrossRef]

124. Ding, X.; Chen, X.; Chen, X.; Zhao, X.; Li, N. A QCM humidity sensor based on fullerene/graphene oxide nanocomposites with high quality factor. *Sens. Actuators B Chem.* **2018**, *266*, 534–542. [CrossRef]

125. Qi, P.; Zhao, C.; Wang, R.; Fei, T.; Zhang, T. High-performance QCM humidity sensors using acidized-multiwalled carbon nanotubes as sensing film. *IEEE Sens. J.* **2018**, *18*, 5278–5283. [CrossRef]

126. Chappanda, K.N.; Shekhah, O.; Yassine, O.; Patole, S.P.; Eddaoudi, M.; Salama, K.N. The quest for highly sensitive QCM humidity sensors: The coating of CNT/MOF composite sensing films as case study. *Sens. Actuators B Chem.* **2018**, *257*, 609–619. [CrossRef]

127. Wu, Z.; Zhu, S.; Dong, X.; Yao, Y.; Guo, Y.; Gu, S.; Zhou, Z. A facile method to graphene oxide/polyaniline nanocomposite with sandwich-like structure for enhanced electrical properties of humidity detection. *Anal. Chim. Acta* **2019**, *1080*, 178–188. [CrossRef] [PubMed]

128. Qi, P.; Zhang, T.; Shao, T.; Yang, B.; Fei, T.; Wang, R. A QCM humidity sensor constructed by graphene quantum dots and chitosan composites. *Sens. Actuators B Chem.* **2019**, *287*, 93–101. [CrossRef]

129. Ren, X.; Zhang, D.; Wang, D.; Li, Z.; Liu, S. Quartz crystal microbalance sensor for humidity sensing based on layer-by-layer self-assembled PDDAC/graphene oxide film. *IEEE Sens. J.* **2018**, *18*, 9471–9476. [CrossRef]

130. Zhang, D.; Wang, D.; Zong, X.; Dong, G.; Zhang, Y. High-performance QCM humidity sensor based on graphene oxide/tin oxide/polyaniline ternary nanocomposite prepared by in-situ oxidative polymerization method. *Sens. Actuators B Chem.* **2018**, *262*, 531–541. [CrossRef]

131. Wang, S.; Xie, G.; Su, Y.; Su, L.; Zhang, Q.; Du, H.; Tai, H.; Jiang, Y. Reduced graphene oxide-polyethylene oxide composite films for humidity sensing via quartz crystal microbalance. *Sens. Actuators B Chem.* **2018**, *255*, 2203–2210. [CrossRef]

132. Wang, L.; Yu, Y.; Xiang, Q.; Xu, J.; Cheng, Z.; Xu, J. PODS-covered PDA film based formaldehyde sensor for avoiding humidity false response. *Sens. Actuators B Chem.* **2018**, *255*, 2704–2712. [CrossRef]

133. Rahimi, R.; Ochoa, M.; Ziaie, B. Comparison of direct and indirect laser ablation of metallized paper for inexpensive paper-based sensors. *ACS Appl. Mater. Interfaces* **2018**, *10*, 36332–36341. [CrossRef]

134. Safari, S.; Van De Ven, T.G.N. Effect of water vapor adsorption on electrical properties of carbon nanotube/nanocrystalline cellulose composites. *ACS Appl. Mater. Interfaces* **2016**, *8*, 9483–9489. [CrossRef]

135. Syrový, T.; Maronová, S.; Kuberský, P.; Ehman, N.V.; Vallejos, M.E.; Pretl, S.; Felissia, E.F.; Area, M.C.; Chinga-Carrasco, G. Wide range humidity sensors printed on biocomposite films of cellulose nanofibril and poly(ethylene glycol). *J. Appl. Polym. Sci.* **2019**, *136*, 47920. [CrossRef]

136. Kano, S.; Fujii, M. All-painting process to produce respiration sensor using humidity-sensitive nanoparticle film and graphite trace. *ACS Sustain. Chem. Eng.* **2018**, *6*, 12217–12223. [CrossRef]

137. Tang, L.; Chen, W.; Chen, B.; Lv, R.; Zheng, X.; Rong, C.; Lu, B.; Huang, B. Sensitive and renewable quartz crystal microbalance humidity sensor based on nitrocellulose nanocrystals. *Sens. Actuators B. Chem.* **2021**, *327*, 128944. [CrossRef]

138. Korottcenkov, G. Electronic and Elctrical Humidity Sensors. In *Hnadbook of Humidity Measurement*; CRC Press: Boca Raton, FL, USA, 2019; Volume 2.

139. Mekawy, M.; Noguchi, H.; Kawakita, J. Quantitative and Qualitative Studies for Real Monitoring of Interfacial Molecular Water. Journal of Colloid and Interface. *Science* **2022**, *613*, 311–319.

140. Tonnesen, M.G.; Feng, X.; Clark, R.A.F. Angiogenesis in Wound Healing. *J. Investig. Derm. Symp. Proc.* **2000**, *5*, 40–46. [CrossRef] [PubMed]

141. Menke, N.B.; Ward, K.R.; Witten, T.M.; Bonchev, D.G.; Diegelmann, R.F. Impaired Wound Healing. *Clin. Dermatol.* **2007**, *25*, 19–25. [CrossRef] [PubMed]

142. Frykberg, R.G.; Banks, J. Challenges in the Treatment of Chronic Wounds. *Adv. Wound Care* **2015**, *4*, 560–582. [CrossRef]

143. Dargaville, T.R.; Farrugia, B.L.; Broadbent, J.A.; Pace, S.; Upton, Z.; Voelcker, N.H. Sensors and Imaging for Wound Healing: A Review. *Biosens. Bioelectron.* **2013**, *41*, 30–42. [CrossRef]

144. McColl, D.; Cartlidge, B.; Connolly, P. Real-time Monitoring of Moisture Levels in Wound Dressings In Vitro: An Experimental Study. *Int. J. Surg.* **2007**, *5*, 316–322. [CrossRef]

145. Brown, M.S.; Ashley, B.; Koh, A. Wearable Technology for Chronic Wound Monitoring: Current Dressings, Advancements, and Future Prospects. *Front. Bioeng. Biotechnol.* **2018**, *6*, 47. [CrossRef]

146. Milne, S.D.; Seoudi, I.; Al Hamad, H.; Talal, T.K.; Anoop, A.; Allahverdi, N.; Zakaria, Z.; Menzies, R.; Connolly, P. A Wearable Wound Moisture Sensor as an Indicator for Wound Dressing Change: An Observational Study of Wound Moisture and Status. *Int. Wound J.* **2016**, *13*, 1309–1314. [CrossRef]

147. Nuutila, K.; Eriksson, E. Moist Wound Healing with Commonly Available Dressings. *Adv. Wound Care* **2021**, *10*, 685–698. [CrossRef] [PubMed]

148. Scott, C.; Cameron, S.; Cundell, J.; Mathur, A.; Davis, J. Adapting Resistive Sensors for Monitoring Moisture in Smart Wound Dressings. *Curr. Opin. Electrochem.* **2020**, *23*, 31–35. [CrossRef]

149. Tessarolo, M.; Possanzini, L.; Gualandi, I.; Mariani, F.; Torchia, L.D.; Arcangeli, D.; Melandri, F.; Scavetta, E.; Fraboni, B. Wireless Textile Moisture Sensor for Wound Care. *Front. Phys.* **2021**, *9*, 722173. [CrossRef]

150. Shamshiri, R.R.; Jones, J.W.; Thorp, K.R.; Ahmad, D.; Man, H.C.; Taheri, S. Review of optimum temperature, humidity, and vapour pressure deficit for microclimate evaluation and control in greenhouse cultivation of tomato: A review. *Int. Agrophys.* **2018**, *32*, 287–302. [CrossRef]

151. Huang, Y.; Li, Y.; Wen, X. The effect of relative humidity on pollen vigor and fruit setting rate of greenhouse tomato under high temperature condition. *Acta Agric. Boreali Occident. Sin.* **2011**, *11*, 1–20.

152. Nepi, M.; Cresti, L.; Guarnieri, M.; Pacini, E. Effect of relative humidity on water content, viability and carbohydrate profile of Petunia hybrida and Cucurbita pepo pollen. *Plant Syst. Evol.* **2010**, *284*, 57–64. [CrossRef]

153. Schoppach, R.; Taylor, J.D.; Majerus, E.; Claverie, E.; Baumann, U.; Suchecki, R.; Fleury, D.; Sadok, W. High resolution mapping of traits related to whole-plant transpiration under increasing evaporative demand in wheat. *J. Exp. Bot.* **2016**, *67*, 2847–2860. [CrossRef]

154. Devi, M.J.; Sinclair, T.R.; Jain, M.; Gallo, M. Leaf aquaporin transcript abundance in peanut genotypes diverging in expression of the limited-transpiration trait when subjected to differing vapor pressure deficits and aquaporin inhibitors. *Physiol. Plant.* **2016**, *156*, 387–396. [CrossRef] [PubMed]

155. Devi, M.J.; Reddy, V.R. Transpiration Response of Cotton to Vapor Pressure Deficit and Its Relationship with Stomatal Traits. *Front. Plant Sci.* **2018**, *9*, 1572. [CrossRef]

156. Vurro, F.; Janni, M.; Coppedè, N.; Gentile, F.; Manfredi, R.; Bettelli, M.; Zappettini, A. Development of an In Vivo Sensor to Monitor the Effects of Vapour Pressure Deficit (VPD) Changes to Improve Water Productivity in Agriculture. *Sensors* **2019**, *19*, 4667. [CrossRef]

157. Alam, S.S.; Islam, A.J.; Hasan, M.M.; Farhad, M.M. Design and Implementation of an Embedded System to Observe the Atmospheric Condition using a Helium Balloon. In Proceedings of the 2018 International Conference on Innovations in Science, Engineering and Technology (ICISET), Chittagong, Bangladesh, 27–28 October 2018; pp. 242–246.

158. Tomita, H.; Cronin, M.F.; Ohishi, S. Asymmetric air-sea heat flux response and ocean impact to synoptic-scale atmospheric disturbances observed at JKEO and KEO buoys. *Sci. Rep.* **2021**, *11*, 469. [CrossRef] [PubMed]